LASER
& PHOTONICS
REVIEWS

Laser Photonics Rev. **11,** No. 2, 1600265 (2017) / **DOI** 10.1002/lpor.201600265

REVIEW ARTICLE

Abstract Whispering gallery modes (WGMs) have been exploited for a broad range of sensing applications. However, the vast majority of WGM sensors consist of passive resonators, requiring complex interrogation systems to be employed, ultimately limiting their practicality. Active resonators containing a gain medium, allowing remote excitation and collection of the WGM-modulated fluorescence spectra, have emerged as an alternative to passive resonators. Although research is still in its infancy, recent progress has reduced the performance gap between the two paradigms, fueled by the potential for new applications that could not previously be realized. Here, recent developments in sensors based on active WGM microresonators are reviewed, beginning with a discussion of the theory of fluorescence-based and lasing WGMs, followed by a discussion of the variety of gain media, resonator architectures, and emerging sensing applications. We conclude with a discussion of the prospects and future directions for improving active WGM sensors.

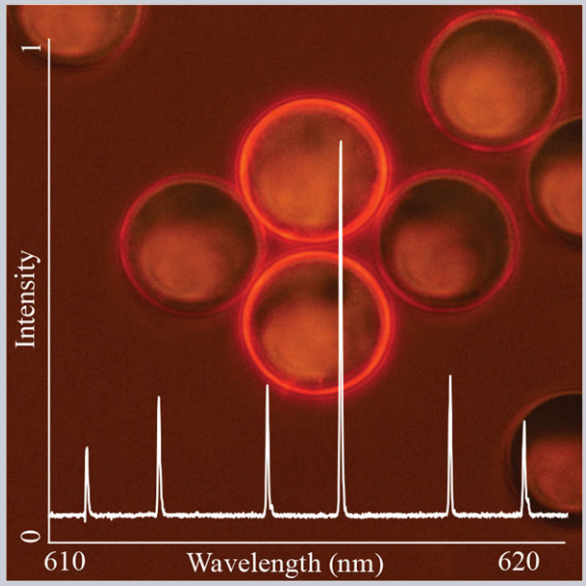

Fluorescent and lasing whispering gallery mode microresonators for sensing applications

Tess Reynolds[1,*], Nicolas Riesen[1,2], Al Meldrum[3], Xudong Fan[4], Jonathan M. M. Hall[1], Tanya M. Monro[1,2], and Alexandre François[1,2,*]

1. Introduction

Whispering gallery modes (WGMs) are optical resonances arising from light being trapped due to total internal reflection at the boundary of a dielectric structure having at least one axis of symmetry. The light propagating along the inner surface of the resonator gives rise to constructive interference when returning in phase after each round trip. This creates resonance features, with spectral positions and linewidths that depend on the dielectric function and geometry of the resonator, as well as the surrounding environment.

Due to their extremely high Quality factor (Q-factor), defined as the ability to store energy, and their small mode volume [1, 2], WGM resonators have found applications spanning sensing [3–5] through to quantum electrodynamics (QED) [6–8] and non-linear optics [9–11]. The applications come with an equal diversity of geometries including spheres [4, 12, 13], hemispheres [14–16], capillaries [17, 18], bubbles [19–21], bottles [22], fibers [23, 24], knots [25, 26], toroids [27, 28], rings [29–31] and disks [32–35]. Materials used for such resonators can be amorphous [4, 12, 36, 37] or crystalline [38–43], and organic or inorganic [18, 29, 44, 45]. The vast majority of resonators studied are passive, requiring an evanescent-wave coupler to interrogate the WGMs. Commonly, these couplers take the form of a tapered optical fiber or a prism, with the taper waist diameter chosen to fulfill the required phase matching conditions [46]. In the case of prism coupling the incidence angle is tuned to achieve the phase matching [47, 48]. For either technique, this allows efficient coupling to the WGMs. Passive resonators have shown tremendous performance, especially in terms of the Q-factor which in some cases can exceed 10^{11} [1], but also in terms of ultra-small mode volumes which is important for QED and non-linear applications. Note however that the requirement for external evanescent coupling configurations, may render any real-life applications outside laboratory environments problematic.

[1] The Institute for Photonics and Advanced Sensing (IPAS), University of Adelaide, Adelaide, SA, 5005, Australia
[2] University of South Australia, Adelaide, SA, 5000, Australia
[3] Department of Physics, University of Alberta, Edmonton, AB, T6G2E1, Canada
[4] Department of Biomedical Engineering, University of Michigan, Ann Arbor, MI 48109, USA
*Corresponding Authors: e-mail: tess.reynolds@adelaide.edu.au; alexandre.francois@unisa.edu.au

In recent years several attempts to reap the performance benefits of passive resonators for real-world applications have emerged. Beyond the more obvious approaches of integrating resonators onto a sensing chip [45, 49, 50], Agarwal *et al.* [51] have integrated a passive silica microsphere at the end of an optical fiber stem with two conical taper couplers, into a monolithic device for dip sensing applications, while Shi *et al.* [52] have directly written, using femtosecond machining, a ring-resonator onto the core of a polished optical fiber. Other researchers have investigated approaches that allow for free space coupling into passive WGM resonators. Ballard *et al.* [53] and Shao *et al.* [54] for instance used deformed microspheres and microtoroids, respectively, presenting "nodes" to couple into, while Zhu *et al.* [55] have used nanoparticles to induce scattering to the same effect. Moreover Zullo *et al.* [56] used a focused free-space edge-coupling scheme to achieve similar results. Using passive free space coupling strategies however comes at the cost of reduced performance.

Active resonators that contain a gain medium are particularly suited to remote excitation and collection of the WGM signal, thereby alleviating some of the practical limitations of typical passive resonators. The first reported active whispering gallery mode resonator was in 1961, barely a year after the first laser was demonstrated by Theodore Maiman. Samarium-doped CaF_2 microspheres were excited by a flashlamp [57], apparently surpassing their lasing threshold at a wavelength of 708.5 nm. In general, upon excitation of the gain medium the emitted fluorescence intensity is modulated at the resonance frequencies as a direct manifestation of the Purcell Effect (*i.e.* increasing the fluorescence intensity at the particular resonance wavelengths) [55, 58, 59].

Fluorescent-based approaches also facilitate the use of smaller resonators thereby in general allowing for greater refractive index sensitivity. Microspheres of 15 μm diameter or even smaller [44], and arrays of resonators can, for example, be interrogated simply by using a scanning microscope [45]. As mentioned active resonators however have reduced Q-factors. The lower Q-factor observed in active resonators is due to several factors. The asphericity can play a significant role for the case of fluorescent microspheres, as shown by Riesen *et al.* [60], who investigated the Q-factor of a dye-doped polymer microsphere measured in free space and through a fiber taper. The asphericity lifts the degeneracy of the resonances in different equatorial planes, so that when indiscriminate collection of these WGMs occurs in free space, the partially overlapping modes effectively result in broader linewidths hence reducing the Q-factor. Similarly, a reduction in the Q-factor of fluorescent cylindrical microcavities has also been observed [61, 62]. As a result, fluorescence-based resonators typically remain somewhat restricted to sensing applications and are unsuitable for non-linear optics and QED applications where high Q-factors and small mode volumes are critical.

For biosensing, single molecule detection has become well established using passive resonators with multiple demonstrations being reported [12, 33, 63–65]. However, since fluorescent resonators have considerably lower Q-factors, and hence higher detection limits, single molecule detection with fluorescent resonators remains challenging. Nonetheless, the free space excitation and collection platform enabled by fluorescent resonators allows for novel applications not possible using passive resonators. For example, free-floating resonators can be inserted into living cells for sensing [66], or for tagging and tracking purposes, using the specific spectral fingerprint of each individual WGM resonator [67, 68]. Even single cells can be turned into WGM resonators by injecting a mixture of fluorescent dye and high refractive index oil, providing the required gain medium to generate the WGMs and also the required light confinement owing to the refractive index contrast between the oil droplet and its surrounding environment [68]. Further, by combining fluorescent microspheres with flow cytometry, automated high-throughput sensing can be achieved using a robust data analysis algorithm to extract real-time information about the resonator's properties from its WGM spectrum [69], while fluorescent cholesteric liquid crystal core shell structures have also shown tremendous potential as magnetically transportable light sources for in-channel illumination applications [70]. In addition, fluorescent resonators can be turned into microscopic laser sources using a lasing gain medium and a suitable pump source, enabling slight enhancements in the Q-factors to be realized upon reaching the lasing threshold [18, 44, 45, 50, 70, 71] and also lowering the detection limit for sensing applications [18, 71].

While there are several review articles on WGMs in the literature covering different aspects such as theory and applications [72, 73], especially related to sensing [3, 5, 74–77] and the growing interest in WGM lasers [78–81], none of them have been specifically dedicated to fluorescent-based resonators and their prospects as sensors. Commonly, fluorescent resonators are covered in a subsection of the review, or only one aspect of their properties is covered such as harnessing unidirectional laser emission from WGM cavities [78] or examining spherical resonators [82], for example. In this review an overview of the recent work on fluorescent-based WGM resonators, which stands as a prolific research field with emerging sensing applications, is provided. First, the basic theory of fluorescent WGMs is discussed, focusing on lasing behavior. Next, strategies for incorporating a gain medium, either organic or inorganic, into resonators and the resulting resonator properties are reviewed, followed by an overview of fluorescent resonator geometries and applications. Concluding remarks focus on future prospects and research opportunities.

2. Fluorescent based and lasing WGM theory

The wavelength positions of all the WGMs in a given resonator are derived using purely geometric arguments, independent of the presence of a gain medium or not, by solving the boundary condition for Maxwell's Equations,

and expanding the electric and magnetic fields of the transverse electric (TE) and transverse magnetic (TM) modes in terms of their eigenfunctions in the appropriate coordinate system (i.e. spherical, cylindrical etc.) [83, 84]. In this standard analytical approach the excitation source is an incident plane wave. However, in order to examine the properties of fluorescent-based resonators alternative excitation sources or resonator structures need to be considered. Most commonly, dipole sources are used as an alternative excitation source as they are analogous to fluorescent dye molecules residing inside a resonator. Even though the excitation source has changed the mode positions of the resonances do not, as these remain a property of both the geometry and refractive index of the resonator and not the excitation source. However, the resulting normalized WGM power spectrum will vary with the number, location and orientation of dipoles present, as was first demonstrated by Chew *et al.* [85, 86]. This has allowed studies into key sensing characteristics such as the refractive index sensitivity and Q-factor of fluorescence based resonators, allowing sensing performance to be optimized [60]. Alternatively, by adjusting the structure of the resonator, i.e. introducing a thin layer of higher refractive index material around the resonator, it is possible to investigate the properties of active resonators, such as quantum dot (QD) coated microspheres [87]. Unlike simply changing the excitation source, by introducing a layer of higher refractive index, the mode positions and resulting refractive index sensitivity change. This can be used to optimize sensing performance as well as explain the observed experimental differences between homogenous and coated spheres [87].

More computationally intensive models such as Finite-Element Method (FEM) [88] or Finite-Difference Time-Domain (FDTD) [89, 90] have yielded complementary results, while also facilitating the investigation of a broader range of resonator shapes [38], as well as providing access to intermediate values of the fields in the time-domain which allows for the study of transient or emergent optical phenomena such as directional emission in deformed cavities [91–95]. Resonator design has also started focusing on microbubbles, and single/multi-layered microspheres [96–99], because of their improved refractive index sensitivity [88, 99] and applications in non-linear optics [11, 100–102].

WGM microcavities have also been used as ultra-low-threshold microlasers in various configurations [18, 44, 45, 50, 70, 74, 103, 104]. Examples of the typical behavior of lasing WGMs in fluorescent resonators can be seen in Fig. 1 (a) and (b), where the mode intensity increases rapidly above the lasing threshold. The Q-factor also increases upon lasing, typically by approximately fourfold [18, 44].

Employing the Lasing Eigenvalue Problem (LEP) formulation [105, 106], which introduces gain through an imaginary part of the refractive index, the lasing frequency and threshold can be determined numerically [107]. However, modeling how the resonator's Q-factor and effective mode volume (V_{eff}) influence the lasing threshold and how the modes behave above the lasing threshold remains problematic.

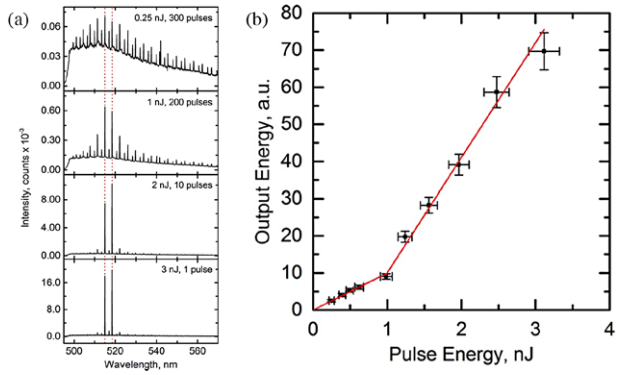

Figure 1 (a) WGM spectra exhibiting the typical transition between fluorescence and stimulated emission regimes of a 10μm in diameter polystyrene microsphere, doped with a green fluorescent protein, inside a living cell and (b) Output energy of the fluorescent WGM signal as a function of the pump power [67]. Reproduced (adapted) with permission from [67]. Copyright (2015), American Chemical Society.

Spillane *et al.* [108] have established a relation for the Raman lasing threshold of a fiber coupled microsphere where the lasing threshold ($I_{threshold}$) scales proportionally with the gain factor (A) and more importantly with V_{eff}/Q^2:

$$I_{threshold} = A\frac{V_{eff}}{Q^2}. \tag{1}$$

The gain factor, A, is related to the Raman gain coefficient for a Raman laser [108], or the gain medium concentration and quantum yield in the case of a fluorescent dye [44]. As expected, the lasing threshold as described in Equation (1), is inversely proportional to the Purcell enhancement factor, F, given by [58],

$$F = 3Q\frac{\left(\frac{\lambda_c}{n}\right)^3}{4\pi^2 V_{eff}} \sim \frac{Q}{V_{eff}}. \tag{2}$$

In other words, a low lasing threshold is achieved if the Purcell factor is high.

However, in earlier work by Sandoghdar *et al.* [109], the lasing threshold of neodymium doped silica microspheres was found to have a linear dependency on Q^{-1}. More recently, Gargas *et al.* [110] established the same Q-factor dependency on the lasing threshold of a ZnO microdisk, further indicating that the behavior of lasing WGMs and especially the lasing threshold is not yet fully understood.

3. Gain media

The most important feature of fluorescence-based resonators, besides the resonator geometry, is the gain medium, which provides the required fluorescence emission that is then modulated by the WGM resonances. In the following section the different types of gain media used are reviewed,

including how they have been incorporated into or combined with WGM resonators. In most cases the approach used for incorporating the gain medium is independent of the resonator geometry itself. The approach used is however strongly influenced by the nature of the gain medium and the resonator material.

3.1. Organic gain media

Fluorescent dyes are the most common gain media used for active microresonators, providing a broad range of emission bands stretching from the UV [111], to the visible and through to the near infrared [112, 113] as shown in Table 1.

A large body of literature exists on the chemistry of various organic dyes in polymer matrices [114], in which the dye chemistry (*i.e.*, solubility, reactivity, and so on) can be classified on the basis of the presence of azo (–N = N–) groups, quinone groups (anthraquinone dyes), or phthalocyanines. Organic fluorophores are commonly mixed with a polymer (*e.g.* PMMA, SU8, PDMS, Polystyrene), and then fabricated into rings, disks [31, 35, 115], solid or liquid microspheres [116], or drawn into solid fibers or capillaries [117, 118]. Alternatively, fluorescent dyes can be introduced into already-formed polymer microresonators. A common method, especially for polystyrene microspheres is to use a two phase liquid system where the resonators are suspended in an aqueous solution while the fluorophore is dissolved in an organic dye that is not miscible with water [44]. Alternatively, resonators can simply be coated with fluorescent dye molecules using chemical moieties on both the dye and the resonator surface [119, 120].

Fluorescent dyes were pivotal in the development of lasing WGM microcavities with thresholds as low as a few tens of nJ/mm^2 [31, 121] to a few μJ/mm^2 [35]. It should be noted that the lasing threshold is strongly influenced by the fluorescent dye quantum yield, concentration and the resonator configuration (Q-factor and mode volume) [31]. Ultimately, the fluorescent dye concentration must be carefully controlled in order to minimize the lasing threshold [44]. Fluorescent dye-doped polymers tend to be plagued by instabilities associated with photochemical degradation under lasing conditions (commonly referred to as "photobleaching") [122], eventually resulting in loss of optical gain. This is a notable limitation in the application of active biosensing devices. Fluorescent dyes are typically excited with pulsed lasers not only to reach the lasing threshold, but also in order to minimize deleterious photochemical effects (*i.e.*, dye-dye or dye-oxygen [123] interactions) and to reduce the formation of nonradiative triplet states [124].

Alternatively, conjugated polymers can be used which are naturally fluorescent and are known to lase [124]. They typically consist of alternating single and double bonded C atoms, producing an electronic structure with extensive orbital delocalization and semiconductor-like energy gap. Conjugated polymer devices can be especially sensitive to the surrounding environment in terms of changes in the lasing intensity or threshold, for example showing "amplified quenching" due to their relatively high carrier mobility. This property makes them sensitive turn-off sensors for nitro compounds [125]. Thus, conjugated polymers could be used for fabricating new and ultra-sensitive resonators for sensing vapors of toxic or dangerous substances, similar to how the lasing intensity of plasmonic cavities is quenched by nitroaromatics [126]. However, the synthesis of WGM-compatible structures from conjugated polymers is difficult [127] without blending with another polymer. Kushida *et al.* [128] were among the first to exploit blends of conjugated polymer, with one donor and one emitter, enabling Fluorescent Resonant Energy Transfer (FRET). A FRET approach could be highly beneficial for limiting photobleaching using adequate donor/acceptor pairs [129], paving the way to a WGM FRET laser [130, 131].

Fluorescent proteins have also been exploited as gain media for active resonators [132]. Jonáš *et al.* [133] for instance demonstrated the potential of liquid microdroplet resonators, doped with suspended fluorescent proteins, as optofluidic biolasers. They revealed that even a single fluorescent bacterium, producing this fluorescent protein, is sufficient for inducing lasing. Chen *et al.* [134] used the fluorescent properties of chlorophylls to develop the first optofluidic chlorophyll laser, laying the path for future biocompatible and biodegradable lasers.

3.2. Inorganic gain media

Inorganic gain media allow continuous wave laser excitation and are relatively impervious to photobleaching. They are chemically robust, stable and offer several accessible excitation wavelength windows, depending on their energy level structure, as shown in Table 2.

Owing to the commercial availability of Quantum Dots (QDs) [135], semiconductors have risen as a popular gain medium. Unlike organic fluorophores where the pump wavelength must be in a specific region of the optical spectrum (*i.e.* the maximum absorption wavelength), the only requirement for exciting semiconductor materials is for the pump wavelength to be shorter than the band gap. Furthermore, as varying the size of the QDs provides control over the fluorescence emission, and since QDs can all be excited with a single pump source, multiplexed sensing is readily achievable [136]. The QDs can be covalently attached [137], grown onto the resonator surface [138] or embedded within the resonator itself [139]. More recently, semiconductor oxides such as ZnO [140, 141] and TiO_2 [142] have been exploited for their light emitting properties. Alternatively, quantum well heterostructures can be used for the fabrication of disk or pillar resonators using state-of-the-art fabrication processes [34, 143, 144], allowing them to be in some cases electrically driven [144] instead of using light for excitation. Lasing using semiconductors has been demonstrated with both quantum well heterostructures [50] and QDs [143, 145]. However,

Table 1 Examples of organic dye-doped resonators

Dye	Excitation/Emission Wavelength (nm)	Resonator Type
CY-3	480/540	Dye-doped SU8 microring [31][a]
Coumarin 540	420/530	Dye-doped liquid droplet [243][a]
Coumarin 6G	480/510	Dye-doped polystyrene microsphere [66, 173]
CY-3	480/540	Dye-doped SU8 microring [31][a]
Yellow Venus protein	500/530	Liquid droplet [133][a]
Rhodamine B	532/580-600	
		Dye-doped monolithic microdisk [115][a]
		Dye-doped melamine-formaldehyde resin microsphere [40]
		Dye-doped solid and hollow PMMA fibers [117, 118][a]
		Dye-doped liquid crystal droplet [244]
		Dye-doped SU8 photoresist [35][a]
Rhodamine 6G	532/580-600	
		Liquid filled microcapillary [113][a]
		Free floating liquid droplet [116], methanol droplet in PDMS matrix [245]
		Dye-doped SU8 microring [31][a]
		Dye-coated rolled microtube [120]
Nile Red	532/580-600	
		Dye-doped polystyrene microsphere [44, 71, 218][a]
		Dye-doped polymer coating on microcapillary [246][a]
		Dye-doped oil droplets [68, 247][a]
CY-5	570/760	Dye-doped SU8 microring [31][a]
DCM	490/600-800	Micro hemisphere [248]
Rhodamine 640 perchlorate	620/700	Liquid droplet [165][a]
Chlorophyll	430/680-730	Liquid filled microcapillary [134][a]

[a]Lasing of the WGM(s) was observed.

non-radiative Auger recombination, exhibiting a recombination rate significantly higher than radiative transitions can drastically reduce the efficiency of such gain media for lasing applications [146, 147].

Perovskite is an emerging new type of gain medium, which refers to crystalline materials with a composition ABX_3, where A and B are two cations and X is an anion bonding to both A and B, such as $CsPbBr_3$. The chemical composition dictates the bandgap structure [148] (*i.e.* direct or indirect bandgap) as well as its emission wavelength [149]. Various perovskites have been used to fabricate micron-sized polygonal resonators (*i.e.* squares, pentagons, or hexagons) supporting WGMs. Lasing of perovskite resonators has also been demonstrated, however the lasing threshold ranges from the relatively high values of a few $\mu J/cm^2$ [150] to tens of $\mu J/cm^2$ [38] owing to the lower Q-factor exhibited by these polygonal resonators.

Rare-earth ions such as Er^{3+}, Nd^{3+} and Tm^{3+}, utilized for telecom fiber amplifiers and fiber lasers, have been used for microsphere fabrication by melting rare-earth doped fused silica fiber to realize microspheres with high Q-factors [151, 152]. Rare-earth ions can also be dissolved in different glass hosts, such as ZBLAN [153] or tellurites [154], unlocking different emission wavelength windows, especially in the mid-infrared where silica's absorption becomes an issue. Upconversion has also been exploited for rare-earth systems, enabling fluorescence emission [155, 156] and lasing [156, 157] at shorter wavelengths. The use of rare earth doped sol-gel coatings has been investigated for coating fused silica microspheres [152, 158]. This method has also been applied to other resonator geometries such as toroids, taking advantage of their low mode volume and large Q-factor, for lasing applications [74, 157]. Many of the fundamental characteristics of WGM-based lasing have been carefully investigated using rare-earth

Table 2 Examples of inorganic material used as gain medium in microcavities

Material	Excitation/Emission Wavelength (nm)	Resonator Type
ZnO	355/390	Hexagonal shaped sub-micron disk [110],[a] Microwire [141, 249],[a] Microsphere [140, 250]
GaN/InGaN	360/366–416	Core-shell wire [251]
CdZnS/ZnS Q dots	395/400	Liquid filled capillary [252][a]
PbI_2	400/∼500	Hexagonal shaped crystal [38][a]
$CsPbBr_3$	520–540	Rectangular cross sectioned nanowire [253][a]
Er^{3+}	997/460–530	Upconversion emission doped microsphere [155], Upconversion lasing on microtoroid [157][a]
Tm^{3+}	1064/450, 461, 784, 802, 816	Upconversion lasing on microtoroid [156][a]
$CH_3NH_3PbBr_3$	400/560	Square shaped microrod [150, 254][a]
CdSe/ZnS Q-dots	433/655	Single Q-dot coating inside thin wall capillary [135][a]
$CsPbX_3$, X = Cl, Br, and I)	400/420-700	Square shaped crystal [149][a]
Si Q-dots	442/770	Q-dot coated capillaries [138]
Nd^{3+}	780/1064	Doped barium titanium silicate microsphere [180],[a] Doped silica microsphere [103],[a] Glass microsphere [181],[a] Doped tellurite microsphere [154][a]
InAs/InGaAs/GaAs instead of InAs/InGaAsGaAs/	532/1270	Microring [143][a]
HgTe Q-dots	830/1240–1780	Q-dot coated microsphere [145][a]
Er^{3+}	980/1535	Doped microtoroid [255],[a] Doped microspheres [152][a]
Tm^{3+}	1550-1610/2000	Microtoroid [74, 160][a]
InAsSb/InAsPSb Quantum well	532/4000	Microdisk [34]

[a]Lasing of the WGM(s) was observed.

doped microsphere systems [159], with CW lasing thresholds ranging from μW [103] to several mW [160].

4. Fluorescent resonator geometries

Microscale resonators have been fabricated from a diverse range of media spanning liquids to polymers, and glass to semiconductors with an equally large variety of geometries. Here we summarize some of the more commonly-utilized fluorescence and lasing WGM resonator geometries and the materials from which they are fabricated.

4.1. Liquid droplets

Microspherical liquid-drop resonators have resurfaced as candidates for microlasers [70, 161] and biosensors [133, 162], despite initial limitations preventing their widespread usage [163]. Liquid droplets form naturally smooth spherical surfaces due to surface tension, allowing high Q-factors to be realized (e.g. 4.2×10^9 at 300 nm) [164]. Fluorescent dye-doped droplet-based resonators have found applications in microfluidics (Fig. 2 (a)) [165], and can also readily be manipulated using optical tweezers [166]. Further, using a water-in-oil-in-water (W/O/W) double emulsion, depicted in Fig. 2(c), where magnetic nanoparticles were incorporated into the center, the droplet's position can be controlled using a magnet [70].

A key advantage of droplet resonators is their ability to be tuned. For example, nematic liquid crystal (LC) droplets [167] provide the means of tuning the WGM resonances using electric fields to manipulate the LC orientations [168], while Tang *et al.* demonstrated the tuning capability via manipulating the diameter of the droplets as they travel into a microfluidic chip and are slowly dissolved [165]. Similar behavior has been reported with self-assembled static dye-doped polystyrene microdroplets formed in a PDMS matrix [169]. Finally, free-floating liquid droplets, shown in Fig. 2 (b), have the capability to change their shape under external stimulus, allowing for tuning of the resonance wavelengths [170].

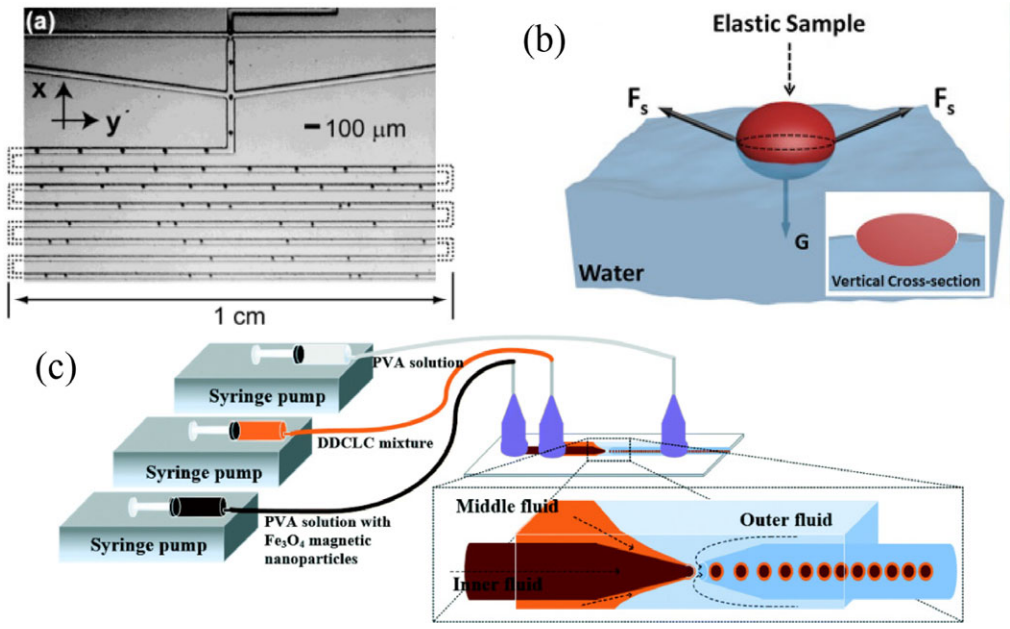

Figure 2 (a) Rhodamine 640 perchlorate doped free-floating benzyl alcohol micro droplets in sodium dodecyl sulfate in a microfluidic chip [165], (b) free floating Rhodamine 6G doped dichloromethane and epoxy resin micro droplet laser [170]. (c) Diagram of glass capillary microfluidic setup for producing W/O/W double-emulsion droplets [70]. (a) Reproduced with permission from [165]. Copyright (2011), Optical Society of America. (b) Reproduced with permission from [170]. Copyright (2016), Nature Publishing Group. (c) Reproduced with permission from [70]. Copyright (2016), Royal Society of Chemistry.

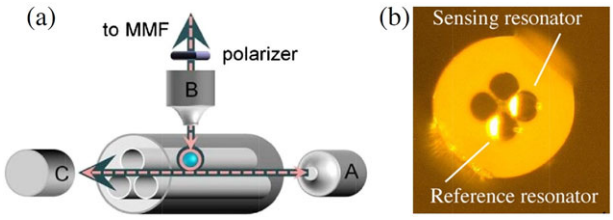

Figure 3 Dye-doped polymer microspheres (a) inside [177] and (b) on the tip [218] of a microstructured optical fiber. (a) Reproduced with permission from [177]. Copyright (2013), Optical Society of America. (b) Reproduced with permission from [218]. Copyright (2016), American Chemical Society.

4.2. Solid microspheres

Solid fluorescent microsphere resonators [69, 128, 171] are commonly fabricated from polymers due to their low cost, structural flexibility and ease of fabrication and integration of a gain medium [44, 128, 169, 172–174]. Beyond the straightforward approach of using a single microsphere resonator, either trapped with optical tweezers [175] or simply deposited onto various substrates [173], there has been interest in combining fluorescent microspherical resonators with capillaries [176], or microstructured optical fibers (MOF) [71, 177, 178], as shown in Fig. 3 (a) and (b). The latter approach allows the fiber to be used to simultaneously excite and collect the fluorescent/lasing WGM signal. Further, the local environment of a MOF around a fluorescent microsphere can enhance specific modes due to a change in mode out-coupling and, as well as an alteration of the dipole emission due to the change in the local environment, with the latter also resulting in an improved lasing efficiency [179]. The combination of a MOF and a fluorescent microsphere can for instance be used for sensing applications, whereby the microsphere resides in one of the fiber's axial holes [71].

Rare-earth doped microspheres are also commonly used although most of the research undertaken with such resonators still employs a fiber taper for evanescent coupling. In comparison, the few free space coupled experiments reported in the literature have displayed lower performance [155, 180, 181], although some interesting opportunities have still been identified notably by Kishi *et al.* who introduced a "terrace" structure, which breaks the microsphere symmetry to achieve quasi-single mode output lasing [154].

4.3. Polygon resonators

Polygons can also support WGMs, and have recently become an interesting addition to more traditional circularly-symmetric resonator geometries. They are often characterized by their number of facets (m), where $m = 2$ corresponds to a Fabry-Perot cavity and cavities with $m \geq 3$ can support quasi-WGMs [182]. The Q-factor for non-absorptive cavities is given as,

$$Q = \frac{m\pi n D sin\left(\frac{2\pi}{m}\right) R^{m/4} \upsilon_0}{2c\left(1 - R^{m/2}\right)}, \quad (3)$$

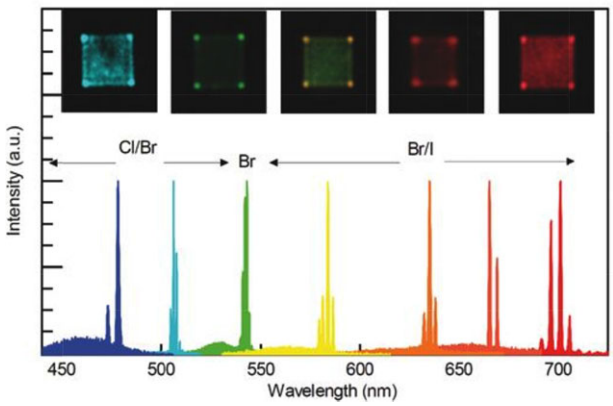

Figure 4 Cesium lead halide ($CsPbX_3$; X = Cl, Br, I) square nanocrystals exhibiting WGM lasing at different wavelengths [149]. Reproduced with permission from [149]. Copyright (2016), Wiley.

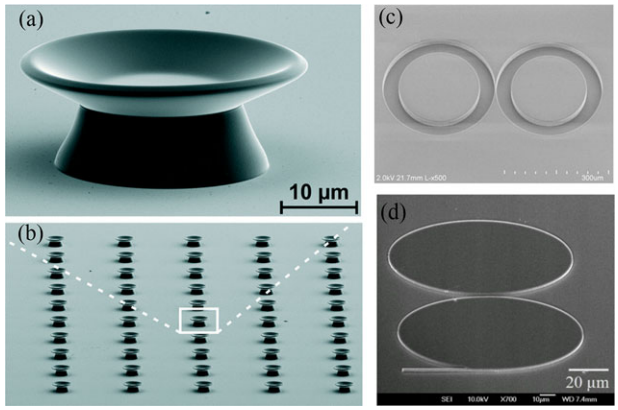

Figure 5 (a), (b) Fluorescent PMMA goblet resonators on a chip [45]. (c) Coupled ring resonators etched on fused silica and coated with a fluorescent dye-doped high refractive index polymer [31] and (d) coupled disk resonator with a protruding waveguide for directional emission [35]. (a), (b) Reproduced with permission from [45]. Copyright (2015), Royal Society of Chemistry. (c) Reproduced with permission from [31]. Copyright (2015), Nature Publishing Group. (d) Reproduced with permission from [35]. Copyright (2015), Elsevier.

where n is the cavity index of refraction, R is the reflectivity of the polygon facet, D is the polygon diameter, c is the speed of light, and υ_0 is the resonance position. By considering the normalized Q-factor, it can be seen that the Q-factor tends to decrease as m increases, revealing why the vast majority of the facetted crystals supporting WGMs (see Fig. 4), exhibit as few facets as possible [182]. Polygonal resonators are commonly grown using Chemical Vapor Deposition from perovskite, which has a fairly large refractive index (typically above 2 in the visible) [38], providing strong confinement of the WGMs [38, 60, 149]. The Q-factors of these resonators however remain somewhat limited to below $\sim 10^3$.

4.4. Toroid, goblet, microdisk and ring resonators

Microfabrication techniques have also been exploited for producing integrated microresonators, the most well-known example being toroid resonators initially developed by Vahala *et al.* at Caltech [27]. These techniques have since been adapted by many other research groups. Earlier examples of microfabricated WGM resonators include microdisks [32,183] and micro-rings [29,184]. These particular resonant structures have the ability to confine light in ultra-small volumes [185], making them particularly suited to QED and lasing applications. Over the last few years, active variants of toroid or "goblet" resonators [45, 185, 186], disks [45, 185] and ring resonators (Fig. 5) [31] have emerged.

Fluorescent goblet resonators can for instance be integrated into microfluidic chips and interrogated remotely using a scanning confocal microscope [45]. It is envisioned that the large-scale integration of lasing resonant microstructures such as microgoblets could be of high interest for multiplexed sensing, with each individual resonator functionalized for the detection of a specific analyte. However, it should be noted that the requirement of a scanning confocal microscope for interrogating individual resonators could limit the practical implementation of such a configuration. Adding a photo-responsive liquid on top of the goblet resonator, for example, could also enable fast tuning of the lasing wavelength through the elastic deformation of the resonator [186].

Microfabrication techniques have also allowed for the fabrication of coupled resonators, which require both resonators to have almost identical dimensions to ensure spectral overlap of the resonances [187]. Coupled disk and ring resonators have been used to exploit the Vernier effect [188] and have also allowed for the realization of single-mode WGM lasers [31,35]. Microfabrication can also be used for the development of alternative resonator geometries with controlled deformations [35] or with directly connected waveguides for unidirectional emission [35, 189] for integrated photonics applications.

The creation of reusable [190] and reconfigurable [31] ring resonator lasers has recently been demonstrated by Chandrahalim *et al.*, opening up the possibility of realizing photonic devices such as on-chip coherent light sources. The reusability of the resonators was demonstrated through depositing, removing and re-depositing both a dye-doped polymer liquid and solid, while wavelength reconfiguration was demonstrated using a similar process via interchanging the gain medium.

Finally, Sun *et al.* investigated the use of proteins for the fabrication of biocompatible disk resonators, using femtosecond machining [115]. By combining a protein matrix with fluorescent dyes, lasing behavior of the resonator was demonstrated, paving the way for novel biocompatible materials to be used as laser sources.

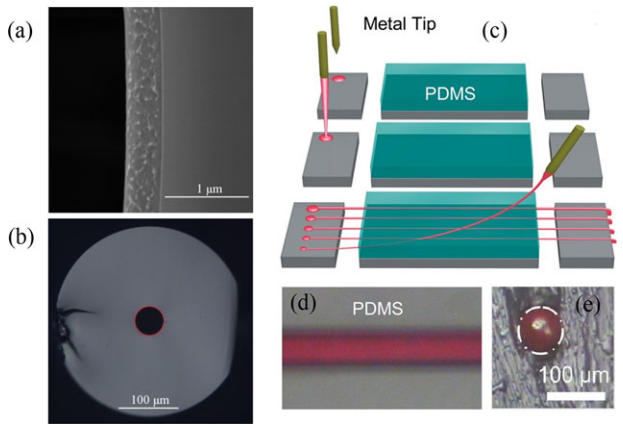

Figure 6 (a), (b) Microcapillaries with a dye-doped polymer coating [246], and (c)-(e) dye-doped polymer fibers [118]. (a), (b) Reproduced with permission from [246]. Copyright (2013), Optical Society of America. (c), (d) and (e) Reproduced with permission from [118]. Copyright (2014), American Chemical Society.

4.5. Capillaries and microfibers

Capillary-type structures with fluorescent channel coatings can also support fluorescent WGMs and have been used as refractometric sensors [18, 138, 191, 192] and biosensors [50]. For microcapillaries to function as active WGM-based sensors, the capillary must be coated with a fluorescent layer that: (a) has a high refractive index in order to support WGMs, and (b) has a thickness of less than $\sim 1\ \mu$m (Figs. 6(a) & (b)) so that the resonant field profile extends sufficiently far into the channel medium. Recently, the first capillary-based WGM laser sensor for refractometric sensing was developed using a dye-doped polymer [18], in principle yielding an order of magnitude improvement in the limit of detection, as compared to the same device operated below the lasing threshold.

Microfibers supporting WGMs such as R6G-doped PMMA [24, 118] or CdSe–ZnS core–shell QD-doped polyvinylpyrrolidone (PVP) nanowires [139], forming cylindrical structures whose diameter can be precisely controlled, are shown in Figs. 6 (c), (d) & (e). Such structures can exhibit lasing WGMs with unusually high refractive index sensitivities of up to 300 nm/RIU [24]. Inkjet-printed fluorescent dye-doped epoxy resin, and PDMS fibers have also been shown to support WGM lasing with good sensitivity to external strain [118, 169, 170], generating interest due to their high flexibility. Fluorescent dye-doped polymer-coated waveguides have similar benefits and are suitable candidates for future biosensing applications [31].

Developments in nanofabrication techniques [193] have enabled the realization of self-rolled nanotubes from bi-layer materials [194–197]. The bi-layer is strained and deposited atop of a sacrificial substrate, which is subsequently etched away, releasing the layer and allowing it to roll and form a nanotube [193]. Most commonly the bi-layer is SiO/SiO_2, enabling robust, transparent and biocompatible sensors to be fabricated [194, 195]. Moreover, hybrid polymer/oxide/polymer tubes have also been fabricated [196], and novel composite cavities made from dielectric and metal materials have also recently been proposed [197]. The diameter and wall thickness of nanotubes can be controlled during the deposition process, and there is also the possibility of incorporating a thin organic active layer [194]. These structures have proven to be successful candidates for refractive index sensors, with sensitivities as high as 450 nm/RIU reported [195]. They have also been shown to allow for the detection of volatile organic compounds [194], could serve as humidity sensors [196], and also present great promise for lab-on-chip integration due to their compact size.

5. Applications

WGM resonators are inherently suited to optical sensing due to the dependence of the spectral positions of the resonances on both the resonator geometry and the refractive index of the surrounding environment. This has been exploited for sensing pressure, temperature, humidity, electric fields, and for biological sensing. Mode tracking is by far the most common interrogation method as depicted in Fig. 7(a), where the resonance shift ($\Delta\lambda$) is directly proportional to the change of effective radius (ΔR) experienced by the resonator as a result of molecular adsorption, local change of refractive index at the resonator surface or the expansion/compression induced by temperature change or isotropic mechanical forces. Unidirectional mechanical strain as depicted in Fig. 7(b) will induce a deformation of the resonator, thereby lifting the mode degeneracy, resulting in a splitting of the resonances which is only observable with fluorescent/lasing microspheres. For instance, Himmelhaus *et al.*, incorporated fluorescent dye-doped microspheres into living cells, enabling the measurement of biomechanical stress induced during endocytosis and phagocytosis to be analyzed via the resonance splitting of a fluorescent polystyrene microsphere [66]. Variation in the Q-factor (Fig. 7(c)) is a common method for monitoring binding events onto passive microspheres [198]. This however requires a very high Q-factor and therefore has never been shown for fluorescent based resonators which typically exhibit lower Q-factor compared with passive resonators. Intensity based sensing provides an alternative sensing modality (Fig. 7(d)), removing the need to continually monitor and track the precise position or linewidth of resonances. In this case the sensitivity, limit of detection, and the dynamic range of the sensor can all be redefined in terms of WGM intensity changes [199, 200]. However, this approach requires for the gain medium to change its emitted intensity as a consequence of the interaction with a specific molecule.

5.1. Physical sensors

In this section we provide a brief overview of physical sensing applications reported in the literature using fluorescent or lasing microresonators. We note here that

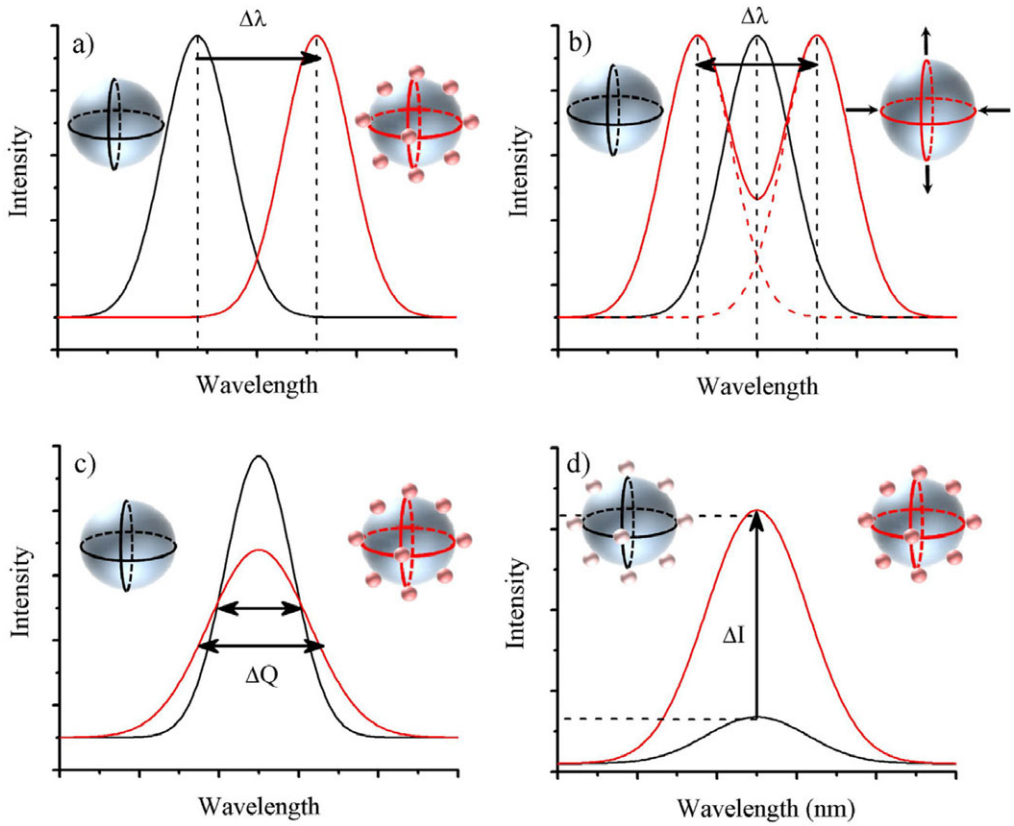

Figure 7 Sensing modalities for fluorescent WGM resonators. (a) Resonance wavelength shift, (b) Mode-splitting, whereby applied stress to the resonator causes the degeneracy in the modes to be lost resulting in a broadening of the WGM peak, (c) variation in the Q-factor, and (d) change in the mode intensity (I).

whilst the performance of most of the active sensors in terms of resolution, sensitivity etc is lower compared to their passive counterparts, the benefits here revolve primarily around the practical advantages of free space interrogation which is readily achieved using active resonators.

5.1.1. Pressure/deformation

Pressure/deformation sensing using active microresonators has been well documented. Martin *et al.*, for instance investigated the effects of pressure on Nd^{3+} doped, barium titanium silicate microspheres, with an average sensitivity of 6.5×10^{-4} GPa^{-1}, which is higher than conventional ruby pressure sensors [201]. Pressure sensing has also been demonstrated with other resonator geometries. For example, Chen *et al.*, used optically pumped dye-doped microfibers encapsulated within PDMS elastomer. Strain-induced refractive index changes from either tensile or compressive forces incurred during bending allows for bidirectional tuning of the WGM resonances, enabling a new range of bend sensing applications [118]. Similarly, Zamanian *et al.*, have demonstrated numerical simulations on the effect of shear stress and wall pressure on the resonances of multiple cylindrical microlasers encapsulated in a slab, allowing for simultaneous wall pressure and shear stress measurement [202]. Finally, Manzo *et al.*, demonstrated the use of a rhodamine 6G doped dome-shaped polymer WGM microlaser with the incorporation of a membrane, for pressure sensing with a resolution as low as 9 Pa [203].

It is worth mentioning here that intrinsically the performance of fluorescent and lasing resonators is not different to passive resonators, although in practice the reduced Q-factors commonly observed in fluorescent resonators can degrade the performance in terms of resolution. However, owing to the free space excitation and collection possible with fluorescent resonators, advantages exist in terms of practicality. One can therefore envision a plethora of other applications which would not be possible with passive resonators requiring a fiber taper or prism for coupling light into the resonator. As an example, Himmelhaus *et al.*, demonstrated the incorporation of fluorescent dye-doped microspheres into living cells, enabling the measurement of cell stress [66].

The slight reduction in performance typical of fluorescent or lasing resonators can therefore be compensated in many cases by the practical advantages afforded to free space interrogation. As with the previous example, the free space excitation also allows for smaller resonators of higher sensitivities to be addressed which would otherwise be

cumbersome if not impractical using taper or prism coupling setups.

5.1.2. Temperature

Active whispering gallery microresonators have also found applications in temperature sensing. For example SBN Er^{3+}-Yb^{3+} co-doped glass microspheres were demonstrated for temperature sensing in the range of 290–380 K [155]. Excitation of the microspheres at a wavelength of 1 μm led to a broad upconversion emission in the green, which is modulated by the sphere resonances, yielding a resonance shift resolution of 4.7 pm/K with a minimum temperature resolution of about 0.01 K [155]. Furthermore, microbottle lasers fabricated from Er:Yb glass molten onto silica capillaries were demonstrated by Ward *et al.* for the same purpose, with the Er:Yb doped outer glass pumped at a wavelength of 980 nm via a taper, while the WGMs were recorded at ~1535 nm. This structure allows for thermo-optic tuning of the microlaser modes by passing gas through the capillary, exploiting the cooling effect that shifts the WGMs to shorter wavelengths. A tuning of the lasing modes was demonstrated over 70 GHz. The setup can also be used to measure liquid flow rate, and a water flow rate sensitivity of 1 GHz/nL/s was demonstrated. Alternatively, the bottle resonators could be calibrated to allow for gas flow rate or indeed temperature measurements by monitoring the WGM shifts [204]. Although this particular example uses a fiber taper for pumping the gain medium and collecting the lasing WGM signal, one can clearly envision the use of a free space approach for this application. We note here that phase transitions in dye-doped LC droplets, resulting in a change of the resonator Q-factor can also be exploited for temperature sensing, although they typically exhibit a very small dynamic range of a few degrees around the LC phase transition [168].

5.1.3. Humidity

Labrador-Paez *et al.*, have demonstrated a liquid-state WGM resonator that allows for highly sensitive humidity sensing. The microdroplets used consist of glycerol doped with rhodamine 6G. Since glycerol is highly hygroscopic the refractive index and radius of the microdroplets change with humidity, resulting in shifts in the resonance wavelength positions. The sensors allow for a relatively high sensitivity of 10^{-3} per relative humidity percent ($\%\ RH^{-1}$) [116].

5.2. Biosensing applications

Since the first demonstration of the capabilities of WGM resonators for label-free biological sensing, measuring either the wavelength shift [4] or Q-factor spoiling [198] upon adsorption of biological molecules onto the resonator surface, significant effort has been invested into improving the sensitivity, selectivity, detection limit and response time of such sensors. While single molecule detection has been achieved with passive resonators providing a gateway for investigating fundamental processes in biology on the nanoscale, single molecule detection is of limited relevance for the vast majority of biosensing applications and especially for medical diagnostics, where biomarkers such as proteins are usually found in concentrations ranging from a few ng/mL [205] to hundreds of μg/mL [206].

Active resonators on the other hand offer novel opportunities not possible with passive resonators, as well as providing another modality for sensing beyond tracking the resonance shift or Q-factor spoiling, namely monitoring WGM intensity changes [200]. The intensity of WGM laser emission originating from active resonators is extremely sensitive to changes in absorption, scattering, and fluctuations in refractive index, all of which can be tailored to monitor specific interactions for a range of biosensing applications [162]. Of course, intensity-based sensing can only be achieved if photobleaching or other changes within the lasing medium itself are minimized or eliminated entirely.

5.2.1. Refractive index biosensing

Refractive index sensing is still the most common WGM sensing application, in which changes in the refractive index (δn) within the WGM evanescent field induce shifts ($\delta\lambda$) in the resonance wavelengths:

$$\frac{\delta \mathrm{n}}{\mathrm{n}} = \frac{\delta\lambda}{\lambda} \,. \tag{4}$$

The wavelength shift induced by adsorption of molecules with excess polarizability (α_{ex}) and a surface density (σ_s) is given by [4],

$$\frac{\delta\lambda}{\lambda} = \frac{\alpha_{ex}\sigma_s}{\varepsilon_0\left(n_1^2 - n_2^2\right)R} \,, \tag{5}$$

where ε_0 is the vacuum permittivity, R is the radius of the resonator, and n_1 and n_2 are the refractive indices of the resonator and the surrounding medium, respectively. The excess polarizability can be approximated from the Clausius-Mossotti equation, in which the polarizability is linearly proportional to the molecular weight. It follows that the sensitivity (S) is strongly dependent on the molecular weight of the molecule to be detected, as is the case for other refractive-index-based sensing techniques.

Here, the sensitivity S depends on the fraction of energy of the WGM contained within the sensing medium [207, 208]. Therefore, increasing the magnitude of the evanescent part of the field through controlling the resonator diameter or the refractive index contrast between the resonator and its surrounding environment, naturally affects the sensitivity [60]. Alternatively, depositing a thin layer of high refractive index material onto the resonator surface can shift the mode field profile in such a way as to

enhance S [99]. Depositing a monolayer of QDs onto the surface of polystyrene microspheres has also been shown to increase the sensitivity [209], but this also reduces the Q-factor. As the magnitude of the evanescent field increases, the Q-factor drops [60], which increases the detection limit [210]. Consequently, an appropriate tradeoff between the sensitivity and the Q-factor needs be made to optimize the sensing performance [60]. Lasing microresonators are highly beneficial in this context, providing a way to significantly increase the Q-factor [18,44,45,50,70,104] without affecting S, and thus significantly lowering the detection limit [18,71]. Another way to improve S is to use coupled resonators, utilizing the Vernier effect in coupled microspheres [211] or microcapillaries, with the latter example resulting in a sensitivity above 2510 nm/RIU [212]. One application of the Vernier effect in two coupled polymer microfibers resulted in a twofold increase in the sensitivity compared with the individual resonators [213].

The vast majority of the literature relating to WGM resonators for biosensing applications focuses on characterizing the sensitivity of the device. Table 3 provides a non-exhaustive overview canvasing the performance of both active and passive resonators from the literature in terms of the sensitivity, Q-factor and detection limit. Although the detection limit of passive sensing configurations may be lower than that of active ones, the practical advantages of active sensing configurations remains unmatched [44,66–70,133,134,144].

Beyond simply characterizing a bulk refractive index change, WGM resonators have also been used for detecting various biomolecules. Bioreceptors, including antibodies [214], aptamers [215], and DNA strands [216,217] have been immobilized onto WGM resonator surfaces. As proof-of-concept demonstrations of active biosensors, the highly specific interaction of streptavidin and biotin/biotinylated proteins has been utilized on a number of devices including, dye-doped polystyrene microspheres [71,218], dye-doped polymer coated microcapillaries [138], polymer microring resonators [219] and polymeric microgoblets [220]. This approach also forms the basis for more complicated surface functionalization approaches, such as the immobilization of biotinylated proteins or antigens. For example, one novel large-scale functionalization technique involves the deposition of fluorescently-labeled phospholipids and the incorporation of biotinylated ink in the procedure. This work demonstrated that microgoblets can be used as biolasers for the detection of anti-2,4-Dinitrophenol [221]. Other examples of biosensing include polystyrene microspheres embedded with CdSe/ZnS QDs for thrombin detection [87], dye-doped polymer coated microcapillaries for detecting Vitamin D Binding Protein [222], fluorescent microspheres for the detection of unlabeled oligonucleotide targets [217], and the multiplexed quantification of ovarian cancer markers [214]. In terms of reaching the same single-molecule detection capability of passive resonators, a self-referenced and self-heterodyned WGM Raman microlaser was recently demonstrated [223]. This setup is restricted in its practical application compared with free space interrogated active resonators, due to the precise alignment, and laser frequency stability and locking requirements.

The capability of a sensor to distinguish or eliminate the effects of non-specific binding is critical for sensing within complex biological samples. Successful prevention of non-specific binding has been demonstrated in passive configurations using covalent surface functionalization strategies, notably using polyethylene glycol (PEG) [224], allowing Pasquardini *et al.* to detect thrombin (down to $\sim 8\ \mu$M) in 10-fold diluted human serum samples [225]. Alternatively, a simpler approach using two active microspheres, with one acting as a floating reference measuring the non-specific binding component, and the second resonator measuring both the non-specific and specific signal has been used for measuring the neutravidin concentration in undiluted human serum [218].

Multiplexed sensing is of particular interest for many biosensing applications, most notably within medical diagnostics whereby multiple markers can be monitored, facilitating better understanding of disease development and diagnosis [226,227]. Multiplexed sensing has been demonstrated with passive resonators, including the remarkable multiplexed DNA sensing by Vollmer *et al.* involving two passive silica microspheres coupled to the same fiber taper [228]. However, the difficulty of positioning more than two microcavities on a single taper and individually tracking the resonances of each cavity is very significant, along with the practical limitations of using a fiber taper as previously discussed. More recently, Genalyte Inc. developed a robust passive multiplexed silicon photonic chip diagnostic platform using ring resonators with integrated waveguides, capable of detecting up to 32 biological analytes from a single sample [229]. Fluorescent resonators also provide the possibility of realizing robust and highly multiplexed biosensors such as the fluorescent-labeled microspheres used by Huckabay *et al.* [230], or the fluorescent microgoblets developed by Wienhold *et al.* [45].

5.2.2. Intensity based biosensing

Intensity based sensing provides an alternative sensing modality, removing the need to continually monitor and track the precise position of resonances. In this case the sensitivity, limit of detection, and the dynamic range of the sensor can all be redefined in terms of WGM intensity changes [199,200]. Figure 7 shows a comparison between the operating principles of an intensity based and resonant-wavelength shift based WGM sensing system. It is clear from Fig. 7 that in an intensity based system the sensitivity becomes strongly dependent on the Q-factor of the resonator, as higher Q-factors result in sharper resonances allowing smaller variations in intensity to be measured. Intensity-based detection systems have also demonstrated higher sensitivities and lower detection limits compared with wavelength-shift sensing methods, albeit with significantly smaller dynamic ranges [219]. By incorporating biochemical/biological molecules directly into the gain medium and taking advantage of the sensitive nature

Table 3 Examples of refractive index sensitivities for active and passive resonators

Sensitivity (nm/RIU)	Q-factor	Detection Limit (RIU)	Resonator Details (passive/active, dimension, refractive index)
1.1 (TM) 0.73 (TE)	2.1×10^8 (TM) 1.7×10^8 (TE)	1.5×10^{-3}	Crystalline (birefringent) magnesium fluoride (MgF_2), 2.4 and 5.8 mm microdisks (n_o = 1.375, n_e = 1.387) [256]
0.5	6×10^7	1.0×10^{-6}	Silica microbubble resonators with diameters 340 μm (n = 1.45) [257]
3	2×10^3	2.6×10^{-2}	Dye-doped polymer coating (1 μm, n = 1.56) inside a 100 μm diameter fused silica capillary [18][a]
6.5	3.0×10^4	6.2×10^{-4}	38 μm diameter barium-titanate microsphere (n = 2.43) excited with a tunable diode laser at 633 nm using a dove prism [37]
7.7	4.5×10^4	5.2×10^{-4}†	9 μm diameter Er doped tellurite microsphere (n = 2.03 at 633 nm) [36]
9.8	800 (Type I) 1500 (Type II)	7.2×10^{-3}	Si Q-dot coated silica capillary (Type I: Inner diameter 25 μm and outer diameter 360 μm, Type II: Inner diameter 100 μm and outer diameter 160 μm) [191]
10	1.5×10^3	4.0×10^{-4}†	Si Q-dot coated silica capillary (50 μm Inner diameter, 360 μm outer diameter) [138]
10	1×10^5	5×10^{-4}	Dye-doped 50 μm diameter PMMA microgoblet (n = 1.48) [45][a]
20	1.2×10^6	1.0×10^{-6}	Silica (n = 1.45) liquid core ring resonator (100 μm outer diameter, 2–3 μm wall thickness) [258]
30	800	10^{-3}	Dye-doped polymer coating (1 μm, n = 1.56) inside a 50 μm diameter fused silica capillary [246]
33	1.3×10^7	8.7×10^{-6}	50 μm diameter PMMA microgoblet (n = 1.48) [220]
50	7×10^4	8×10^{-5}	10 μm diameter dye-doped polystyrene microsphere [44][a]
50	2×10^4	2.6×10^{-5}	Dye-coated 38 μm diameter soda-lime microsphere emitting at 630 nm [230]
100	10^3 §	4×10^{-4}	CdSe/ZnS quantum dot embedded 10 μm diameter polystyrene microspheres (n = 1.59) emitting at 550 nm [87]
100	1700	1×10^{-4}	Si Q-dot coated 30 μm diameter silica (n = 1.45) microsphere [259]
300	8.2×10^3	-	Dye-doped 36 μm diameter PMMA microfiber (n = 1.48) emitting at 600 nm [24]
390	500	1×10^{-4}	Thin wall silica (n = 1.45) capillary (11 μm outer diameter, 0.8 μm wall thickness) [260]
570	1.2×10^5	2.8×10^{-7}	Thin wall silica (n = 1.45) capillary (70 μm outer diameter, 2–3 μm wall thickness) [261]
5930	2.5×10^3 §	2.7×10^{-5}	Coupled optofluidic ring laser (125 μm diameter, n = 1.52) [262][a]

[a]Lasing of the WGM(s) was observed; † Calculated values of detection limit based on the refractive index sensitivity (S) and Q-factor, assuming a wavelength resolution of 4 pm achievable with a high-resolution spectrometer; § Calculated values of the Q-factor from the WGM spectrum.

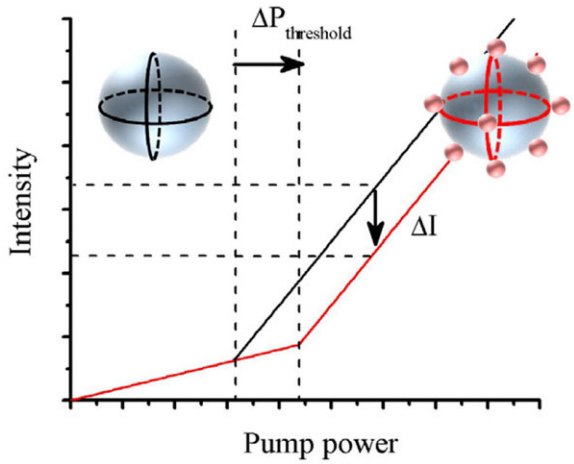

Figure 8 Variation of lasing characteristic induced by molecular adsorption resulting in a change in the lasing threshold ($P_{threshold}$) and mode intensity (I).

of the lasing threshold on the resonator parameters or environment, optofluidic biolasers have emerged as a highly effective platform for a range of biosensing applications [162]. Capillary-based sensors, such as optofluidic ring-resonators or fluorescent-core microcapillaries, are particularly interesting with their ability to blend together microfluidics and laser technology, alleviating complexities involved with sample delivery. For example, Sun *et al.* incorporated DNA samples and probes into the gain medium which is delivered through the channel of an optofluidic ring-resonator, allowing sensitive and selective detection of two different DNA sequences [231].

Alternatively, recent work by Chen *et al.* demonstrated the ability to position the gain medium onto the surface of the resonator, producing an optofluidic laser with a single molecular layer of gain, opening up the possibility for surface-based detection, a feature that is not commonly observed in optofluidic lasing platforms [232].

6. Conclusion and future prospects

Despite many emerging sensing applications, the performance of active resonators remains significantly lower than their passive counterparts. Fluorescent-based resonators typically exhibit a lower Q-factor which can constrain the sensor detection limit, despite lasing of the WGMs of such resonators potentially allowing for a slight improvement of both the Q-factor and signal to noise ratio. Nevertheless, there are many avenues worth exploring that could enable the emergence of applications exclusive to active resonators.

One envisioned approach combines fluorescent resonators with plasmonic effects. While plasmonic nanoparticles have been successfully used to reach single molecule detection [12,233] and passive resonators have been coated with a metal layer to induce a WGM-like behavior of the plasmonic wave [234], the adaptation of the same methodologies to fluorescent resonator has not yet been investigated. Even more interesting is the prospect of using another plasmonic effect, namely Metal Enhanced Fluorescence (MEF), which is well suited to lasing microresonators. MEF is attributed to the stronger interactions occurring between a fluorophore's excited states and the induced surface plasmon resonances (SPR) in metal particles or films due to the increased electromagnetic field in the proximity of metal [235]. As a result, the radiative fluorescence lifetime can be drastically decreased, resulting in an enhancement of the fluorescence intensity. This phenomenon is obviously of particular interest for fluorescent/lasing-based microresonators, potentially driving down the lasing threshold. However, MEF also has very strict requirements. First, the SPR must match the excitation wavelength of the gain medium. Most of the noble metals used for their plasmonic properties (Au, Ag) exhibit SPRs in the shorter-wavelength range of the visible spectrum, restricting the gain media that could be used. In addition, MEF requires the gain medium to be positioned a few nanometers above the metal supporting the SPR, in order to produce the maximum enhancement [235]. Therefore, only two options appear to be viable for fluorescent microresonators to benefit from MEF. First, one may coat or incorporate metallic nanoparticles in fluorescent resonators, similar to what has been achieved with plasmonic epitope [12, 233], although one may question the impact this procedure will have on the Q-factor, since these nanoparticles are likely to behave as scattering centers. Second, depositing micron size resonators onto specifically engineered substrates that can support long range SPRs (LRSPRs) [236] may further extend the penetration depth of the plasmonic field, and consequently increase the distance above the metallic coating at which the fluorescence is enhanced.

Enhanced Raman Scattering is another intriguing phenomenon, taking advantage of either the hot spots created by the propagating WGMs at the resonator surface to enhance the Raman effect without the use of metallic nanoparticles (cavity enhanced Raman scattering) [237, 238] or through the addition of nanoparticles inducing scattering at the microresonator surface [239]. Lasing microresonators are of particular interest for exploiting these effects, promising highly sensitive detection modalities. However, these effects require the resonator to exhibit very high Q-factors.

As discussed, simply using the WGM fluorescence intensity for sensing has been widely exploited, relying on the fluorescent/lasing gain medium emission that is varied upon interaction with the analyte to be detected. The Q-factor can also be affected by binding events occurring at the resonator surface, with the first demonstration of this phenomenon being documented over a decade ago by Nadeau *et al.* [198]. More recently, Hu *et al.* theoretically investigated the resonance broadening induced by dielectric nanoparticles and revealed that a single particle can be detected without resorting to any sensitivity enhancement mechanism or active noise control technique [240]. The same mechanism was experimentally used by Shao *et al.* for the detection of a single virus particle [241]. This novel sensing mechanism holds great promise for lasing resonators, as any Q-factor spoiling should also result in an

increase of the lasing threshold as shown in the Fig. 8. Although measuring the lasing threshold could be somewhat impractical, one can resort to measuring only the intensity of the lasing modes, assuming that both the gain medium and pump source intensity are stable. This method would not only allow better performance to be achieved but also alleviate practical requirements related to the specialized and expensive equipment typically used for performing mode tracking measurements, potentially paving the way for a viable commercial application of WGM-based sensing.

Finally, fluorescent microresonators offer the potential for *in-vivo* sensing. After the first demonstration of intracellular sensing [66] and tagging [67, 68], the concept of free-floating resonators inside blood vessels no longer seems quite as unrealistic, especially with the emergence of flow cytometry [161]. However, for this vision to be realized one would have to use a gain medium in the NIR rather than in the visible spectrum [242], as the latter is strongly absorbed by tissue. Powerful spectral analysis methods for the determination and characterization of binding events without prior knowledge of the resonance spectra would be required in such setups.

Acknowledgements. T. M. Monro acknowledges the support of an Australian Research Council (ARC) Georgina Sweet Laureate Fellowship. The authors acknowledge the support of the ARC Centre of Excellence for Nanoscale Biophotonics.

Received: 3 October 2016, **Revised:** 15 December 2016, **Accepted:** 27 February 2017

Published online: 21 March 2017

Key words: Whispering gallery modes, microcavities, fluorescence, laser resonators, sensing.

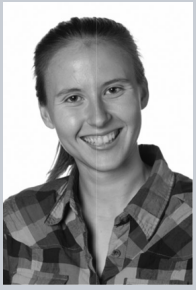

Tess Reynolds is a PhD candidate at the University of Adelaide, Australia. Her research focuses on the development of a fluorescence-based fiber-tip whispering gallery mode biosensing platform from both a theoretical and experimental standing. Previously she has undertaken research in computational astrophysics also at the University of Adelaide.

Nicolas Riesen gained his PhD from The Australian National University in 2014, with his thesis focusing on mode-division multiplexing for increasing optical fiber capacity. Dr Riesen subsequently worked as a research associate at the University of Adelaide in Australia. Currently he is a research fellow at the University of South Australia, where he is involved in the study of a variety of optical phenomena in whispering gallery mode resonators.

Al Meldrum is a full professor at the University of Alberta, Canada, where he currently holds a Vargo Teaching Chair. He has more than 150 publications in physics, chemistry, materials science, optics, physics education, and earth science journals. Currently he focuses on optical cavities, optical sensors, fluorescence imaging and spectroscopy, and the basic physics of cavity-quantum-dot interactions.

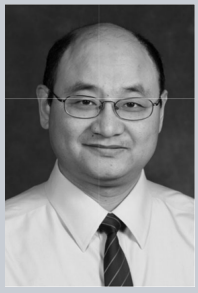

Xudong Fan obtained his PhD in physics and optics from the University of Oregon in 2000. Currently, he is a Professor at the University of Michigan and serves on the Editorial Board of Lab on a Chip for the Royal Society of Chemistry and the International Editorial Advisory Board of Advanced Materials Technologies. His research interests include photonic bio/chemical sensors, micro/nano-fluidics, optofluidics, micro-gas chromatography devices, nano-photonics and novel photonic devices, for medical diagnostics. He is a Fellow of the Optical Society of America and the Royal Society of Chemistry.

Jonathan Hall is a physicist at the University of Adelaide, Australia, specialising in computational research, with recent extensive post-graduate training in experimental nanoscale biophotonics. His research interests include resonance spectroscopy, field simulation in finite-volume structures, and applications to biosensing.

Tanya Monro is Deputy Vice Chancellor Research and Innovation and an ARC Georgina Sweet Laureate Fellow at the University of South Australia. Professor Monro is a Fellow of the Australian Academy of Sciences, the Australian Academy of Technological Sciences and Engineering, the Australian Institute of Physics and also an inaugural Bragg Fellow of the Royal Institution of Australia (RiAus). Her main research interests encompass optical fibers technologies, from sensing to non-linear optics and laser physics.

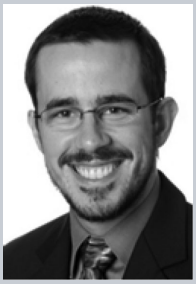

Alexandre François received his PhD in electrical engineering from the University of Sherbrooke, Canada, in 2006. After post-doctoral experience developing fluorescent based whispering gallery mode biosensors for a Japanese pharmaceutical company (Fujirebio Inc.), Dr François joined the University of Adelaide, in 2008 and the University of South Australia in 2015. His research mainly focuses on label free sensing technologies with a specific emphasis on plasmonics and whispering gallery modes.

References

[1] M. Gorodetskii, Y. Demchenko, D. Zaitsev, V. Krutikov, Y. Zolotarevskii, and V. Lyaskovskii, Meas. Tech. **12**, 1386–1395 (2015).
[2] C. Zou, C. Dong, J. Cui, F. Sun, Y. Yang, X. Wu, Z. Han, and G. Guo, Sci Sin-Phys Mech Astron **42**, 1155–1175 (2012).
[3] M. R. Foreman, J. D. Swaim, and F. Vollmer, Adv. Opt. Photon. **7**, 168–240 (2015).
[4] F. Vollmer, D. Braun, A. Libchaber, M. Khoshsima, I. Teraoka, and S. Arnold, Appl. Phys. Let. **80**, 4057–4059 (2002).
[5] A. François, Y. Zhi, and A. Meldrum, Photonic Materials for Sensing, Biosensing and Display Devices, Vol. 229 (Springer International Publishing, 2016), p. 237–288.
[6] Z. K. Minev, K. Serniak, I. M. Pop, Z. Leghtas, K. Sliwa, M. Hatridge, L. Frunzio, R. J. Schoelkopf, and M. H. Devoret, Phys. Rev. Appl. **5**, 044021 (2016).
[7] J. Volz, M. Scheucher, C. Junge, and A. Rauschenbeutel, Nat. Photon. **8**, 965–970 (2014).
[8] W. Song, W. Yang, Q. Chen, Q. Hou, and M. Feng, Opt. Express **23**, 13734–13751 (2015).
[9] G. D'Aguanno and C. R. Menyuk, Phys. Rev. A **93**, 043820 (2016).
[10] I. Breunig, Laser Photon. Rev. **10**, 569–587 (2016).
[11] N. Riesen, W. Q. Zhang, and T. M. Monro, Opt. Express **24**, 8832–8847 (2016).
[12] M. D. Baaske, M. R. Foreman, and F. Vollmer, Nat. Nano. **9**, 933–939 (2014).
[13] A. Chiasera, Y. Dumeige, P. Feron, M. Ferrari, Y. Jestin, G. Nunzi Conti, S. Pelli, S. Soria, and G. C. Righini, Laser Photon. Rev. **4**, 457–482 (2010).
[14] R. Chen, T. Van Duong, and H. D. Sun, Sci. Rep. **2**, 244 (2012).
[15] V. D. Ta, R. Chen, D. M. Nguyen, and H. D. Sun, Appl. Phys. Lett. **102**, 031107 (2013).
[16] V. D. Ta, R. Chen, and H. D. Sun, Adv. Mater. **24**, OP60–OP64 (2012).
[17] I. M. White, H. Oveys, and X. Fan, Opt. Lett. **31**, 1319–1321 (2006).
[18] A. François, N. Riesen, K. Gardner, T. M. Monro, and A. Meldrum, Opt. Express **24**, 12466–12477 (2016).
[19] M. Sumetsky, Y. Dulashko, and R. S. Windeler, Opt. Lett. **35**, 1866–1868 (2010).
[20] W. Lee, Y. Sun, H. Li, K. Reddy, M. Sumetsky, and X. Fan, Appl. Phys. Lett. **99**, 091102 (2011).
[21] J. M. Ward, N. Dhasmana, and S. N. Chormaic, Eur. Phys. J. **223**, 1917–1935 (2014).
[22] M. Sumetsky, Opt. Lett. **29**, 8–10 (2004).
[23] L. Tong, R. R. Gattass, J. B. Ashcom, S. He, J. Lou, M. Shen, I. Maxwell, and E. Mazur, Nature **426**, 816–819 (2003).
[24] V. Duong Ta, R. Chen, L. Ma, Y. Jun Ying, and H. Dong Sun, Laser Photon. Rev. **7**, 133–139 (2013).
[25] X. Jiang, L. Tong, G. Vienne, X. Guo, A. Tsao, Q. Yang, and D. Yang, Appl. Phys. Lett. **88**, 223501 (2006).
[26] Q. Yang, X. Jiang, X. Guo, Y. Chen, and L. Tong, Appl. Phys. Lett. **94**, 101108 (2009).
[27] D. K. Armani, T. J. Kippenberg, S. M. Spillane, and K. J. Vahala, Nature **421**, 925–928 (2003).
[28] J. Su, A. F. Goldberg, and B. M. Stoltz, Light Sci. Appl. **5**, e16001 (2016).
[29] C.-Y. Chao and L. J. Guo, Appl. Phys. Lett. **83**, 1527–1529 (2003).
[30] M. Sumetsky, R. S. Windeler, Y. Dulashko, and X. Fan, Opt. Express **15**, 14376–14381 (2007).
[31] H. Chandrahalim and X. Fan, Sci. Rep. **5**, 18310 (2015).
[32] S. L. McCall, A. F. J. Levi, R. E. Slusher, S. J. Pearton, and R. A. Logan, Appl. Phys. Lett. **60**, 289–291 (1992).
[33] J. Zhu, S. K. Ozdemir, Y.-F. Xiao, L. Li, L. He, D.-R. Chen, and L. Yang, Nat. Photon. **4**, 46–49 (2010).
[34] Yen-Chih Lin, Ming-Hua Mao, Chen-Jun Wu, and Hao-Hsiung Lin, Optics Letters **40**, 1904–1907 (2015).
[35] S. K. Vanga and A. A. Bettiol, Nucl. Instrum. Methods Phys. Res. B **348**, 209–212 (2015).
[36] Y. Ruan, K. Boyd, H. Ji, A. François, H. Ebendorff-Heidepriem, J. Munch, and T. M. Monro, Opt. Express **22**, 11995–12006 (2014).
[37] S. M. Wildgen and R. C. Dunn, Biosensors **5**, 118–130 (2015).
[38] X. Liu, S. T. Ha, Q. Zhang, M. de la Mata, C. Magen, J. Arbiol, T. C. Sum, and Q. Xiong, ACS Nano **9**, 687–695 (2015).
[39] M. Förtsch, G. Schunk, J. U. Fürst, D. Strekalov, T. Gerrits, M. J. Stevens, F. Sedlmeir, H. G. Schwefel, S. W. Nam, and G. Leuchs, Phys. Rev. A **91**, 023812 (2015).
[40] J. Pfeifle, A. Coillet, R. Henriet, K. Saleh, P. Schindler, C. Weimann, W. Freude, I. V. Balakireva, L. Larger, and C. Koos, Phys. Rev. Lett. **114**, 093902 (2015).
[41] I. S. Grudinin, A. B. Matsko, and L. Maleki, Opt. Express **15**, 3390–3395 (2007).
[42] V. S. Ilchenko, A. A. Savchenkov, A. B. Matsko, and L. Maleki, Phys. Rev. Lett. **92**, 043903 (2004).
[43] I. S. Grudinin, A. B. Matsko, A. A. Savchenkov, D. Strekalov, V. S. Ilchenko, and L. Maleki, Opt. Commun. **265**, 33–38 (2006).
[44] A. François, N. Riesen, H. Ji, S. Afshar V, and T. M. Monro, Appl. Phys. Lett. **106**, 031104 (2015).
[45] T. Wienhold, S. Kraemmer, S. F. Wondimu, T. Siegle, U. Bog, U. Weinzierl, S. Schmidt, H. Becker, H. Kalt, T. Mappes, S. Koeber, and C. Koos, Lab Chip **15**, 3800–3806 (2015).

[46] J. Knight, G. Cheung, F. Jacques, and T. Birks, Opt. Lett. **22**, 1129–1131 (1997).
[47] Y.-L. Pan and R. K. Chang, Appl. Phys. Lett. **82**, 487–489 (2003).
[48] V. B. Braginsky, M. L. Gorodetsky, and V. S. Ilchenko, Phys. Lett. A **137**, 393–397 (1989).
[49] K. A. Knapper, K. D. Heylman, E. H. Horak, and R. H. Goldsmith, Adv. Mater. **28**, 2945–2950 (2016).
[50] M. M. Karow, P. Munnelly, T. Heindel, M. Kamp, S. Höfling, C. Schneider, and S. Reitzenstein, Appl. Phys. Lett. **108**, 081110 (2016).
[51] M. Agarwal and I. Teraoka, Anal. Chem. **87**, 10600–10604 (2015).
[52] L. Shi, T. Zhu, D. Huang, M. Liu, M. Deng, and W. Huang, Opt. Lett. **40**, 3770–3773 (2015).
[53] Z. Ballard, M. D. Baaske, and F. Vollmer, Sensors **15**, 8968–8980 (2015).
[54] L. Shao, L. Wang, W. Xiong, X.-F. Jiang, Q.-F. Yang, and Y.-F. Xiao, Appl. Phys. Lett. **103**, 121102 (2013).
[55] J. Zhu, S. Özdemir, H. Yilmaz, B. Peng, M. Dong, M. Tomes, T. Carmon, and L. Yang, Sci. Rep. **4**, 6396 (2014).
[56] R. Zullo, A. Giorgini, S. Avino, P. Malara, P. De Natale, and G. Gagliardi, Proc. SPIE **9727**, 972713–972713 (2016).
[57] C. G. B. Garrett, W. Kaiser, and W. L. Bond, Phys. Rev. **124**, 1807–1809 (1961).
[58] H. Benisty, C. Weisbuch, J.-M. Gérard, R. Houdré, and J. Rarity, Confined Photon Systems, Vol. 531 (Berlin Springer Verlag, 1999).
[59] T. Baba and D. Sano, IEEE J. Sel. Top. Quantum Electron. **9**, 1340–1346 (2003).
[60] N. Riesen, T. Reynolds, A. François, M. R. Henderson, and T. M. Monro, Opt. Express **23**, 28896–28904 (2015).
[61] S. Afshar V, M. R. Henderson, A. D. Greentree, B. C. Gibson, and T. M. Monro, Opt. Express **22**, 11301–11311 (2014).
[62] M. Sumetsky, Opt. Express **13**, 6354–6375 (2005).
[63] V. R. Dantham, S. Holler, C. Barbre, D. Keng, V. Kolchenko, and S. Arnold, Nano Lett. **13**, 3347–3351 (2013).
[64] S. I. Shopova, R. Rajmangal, S. Holler, and S. Arnold, Appl. Phys. Lett. **98**, 243104 (2011).
[65] M. Baaske and F. Vollmer, ChemPhysChem **13**, 427–436 (2012).
[66] M. Himmelhaus and A. François, Biosens. Bioelectron. **25**, 418–427 (2009).
[67] M. Schubert, A. Steude, P. Liehm, N. M. Kronenberg, M. Karl, E. C. Campbell, S. J. Powis, and M. C. Gather, Nano Lett. **15**, 5647–5652 (2015).
[68] M. Humar and S. H. Yun, Nat. Photon. **9**, 572–576 (2015).
[69] J.-R. Carrier, M. Boissinot, and C. Nì. Allen, Am. J. Phys. **82**, 510–520 (2014).
[70] L.-J. Chen, L.-L. Gong, Y.-L. Lin, X.-Y. Jin, H.-Y. Li, S.-S. Li, K.-J. Che, Z.-P. Cai, and C. J. Yang, Lab Chip **16**, 1206–1213 (2016).
[71] A. François, T. Reynolds, and T. M. Monro, Sensors **15**, 1168–1181 (2015).
[72] A. N. Oraevsky, Quant. Electron. **32**, 377–400 (2002).
[73] K. J. Vahala, Nature **424**, 839–846 (2003).
[74] S. Arnold, S. Holler, and X. Fan, Nano-Structures for Optics and Photonics (Springer, 2015), p. 309–322.
[75] J. H. Wade and R. C. Bailey, Annu. Rev. Anal. Chem. **9**, 1–25 (2016).
[76] F. Vollmer and S. Arnold, Nat. Methods **5**, 591–596 (2008).
[77] Y. Sun and X. Fan, Anal. Bioanal. Chem. **399**, 205–211 (2011).
[78] X.-F. Jiang, C.-L. Zou, L. Wang, Q. Gong, and Y.-F. Xiao, Laser Photon. Rev. **10**, 40–61 (2016).
[79] S. Yang, Y. Wang, and H. Sun, Adv. Opt. Mater. **3**, 1136–1162 (2015).
[80] J. Ward and O. Benson, Laser Photon. Rev. **5**, 553–570 (2011).
[81] L. He, Ş. K. Özdemir, and L. Yang, Laser Photon. Rev. **7**, 60–82 (2013).
[82] S. Soria, S. Berneschi, M. Brenci, F. Cosi, G. Nunzi Conti, S. Pelli, and G. C. Righini, Sensors **11**, 785–805 (2011).
[83] I. Teraoka and S. Arnold, J. Opt. Soc. Am. B **23**, 1381–1389 (2006).
[84] C. C. Lam, P. T. Leung, and K. Young, J. Opt. Soc. Am. B **9**, 1585–1592 (1992).
[85] H. Chew, Phys. Rev. A **38**, 3410–3416 (1988).
[86] H. Chew, J. Chem. Phys. **87**, 1355–1360 (1987).
[87] H. T. Beier, G. L. Coté, and K. E. Meissner, Ann. Biomed. Eng. **37**, 1974–1983 (2009).
[88] Y. Yang, J. Ward, and S. N. Chormaic, Opt. Express **22**, 6881–6898 (2014).
[89] J. M. Hall, V. S. Afshar, M. R. Henderson, A. François, T. Reynolds, N. Riesen, and T. M. Monro, Opt. Express **23**, 9924–37 (2015).
[90] T. C. Preston and J. P. Reid, J. Opt. Soc. Am. A **32**, 2210–2217 (2015).
[91] N. L. Aung, L. Ge, O. Malik, H. E. Türeci, and C. F. Gmachl, Appl. Phys. Lett. **107**, 151106 (2015).
[92] X.-P. Zhan, J.-F. Ku, Y.-X. Xu, X.-L. Zhang, J. Zhao, W. Fang, H.-L. Xu, and H.-B. Sun, IEEE Photonic. Tech. Lett. **27**, 311–314 (2015).
[93] Q. J. Wang, C. Yan, N. Yu, J. Unterhinninghofen, J. Wiersig, C. Pflügl, L. Diehl, T. Edamura, M. Yamanishi, H. Kan, and F. Capasso, Proc. Natl. Acad. Sci. **107**, 22407–22412 (2010).
[94] J. U. Nöckel, A. D. Stone, and R. K. Chang, Opt. Lett. **19**, 1693–1695 (1994).
[95] C. Gmachl, F. Capasso, E. E. Narimanov, J. U. Nöckel, A. D. Stone, J. Faist, D. L. Sivco, and A. Y. Cho, Science **280**, 1556–1564 (1998).
[96] H. Chew, M. Kerker, and P. J. McNulty, J. Opt. Soc. Am. **66**, 440–444 (1976).
[97] W. Liang, Y. Xu, Y. Huang, A. Yariv, J. G. Fleming, and S.-Y. Lin, Opt. Express **12**, 657–669 (2004).
[98] W. Yang, Appl. Opt. **42**, 1710–1720 (2003).
[99] I. Teraoka and S. Arnold, J. Opt. Soc. Am. B **23**, 1434–1441 (2006).
[100] S. K. Biswas and S. Kumar, Opt. Express **23**, 26738–26753 (2015).
[101] Q. Lu, S. Liu, X. Wu, L. Liu, and L. Xu, Opt. Lett. **41**, 1736–1739 (2016).
[102] M. Li, X. Wu, L. Liu, and L. Xu, Opt. Express **21**, 16908–16913 (2013).
[103] Y. Ding, H. Fan, X. Zhang, X. Jiang, and M. Xiao, Opt. Commun. (2016).

[104] S. Yakunin, L. Protesescu, F. Krieg, M. I. Bodnarchuk, G. Nedelcu, M. Humer, G. De Luca, M. Fiebig, W. Heiss, and M. V. Kovalenko, Nat. Commun. **6**, 8056 (2015).
[105] E. I. Smotrova and A. I. Nosich, Opt. Quant. Electron. **36**, 213–221 (2004).
[106] S.-W. Chang, The Current Trends of Optics and Photonics, Vol. 129 (Springer Netherlands, Dordrecht, 2015), p. 361–376.
[107] Y. Huang and Y. Y. Lu, J. Mod. Opt. **61**, 390–396 (2014).
[108] S. Spillane, T. Kippenberg, and K. Vahala, Nature **415**, 621–623 (2002).
[109] V. Sandoghdar, F. Treussart, J. Hare, V. Lefèvre-Seguin, J. M. Raimond, and S. Haroche, Phys. Rev. A **54**, 1777–1780 (1996).
[110] D. J. Gargas, M. C. Moore, A. Ni, S.-W. Chang, Z. Zhang, S.-L. Chuang, and P. Yang, ACS Nano **4**, 3270–3276 (2010).
[111] M. Gupta, D. K. Maity, S. K. Nayak, and A. K. Ray, J. Photochem. Photobiol. A **300**, 15–21 (2015).
[112] O. Redy-Keisar, K. Huth, U. Vogel, B. Lepenies, P. H. Seeberger, R. Haag, and D. Shabat, Org. Biomol. Chem. **13**, 4727–4732 (2015).
[113] G. Niu, W. Liu, J. Wu, B. Zhou, J. Chen, H. Zhang, J. Ge, Y. Wang, H. Xu, and P. Wang, J. Org. Chem. **80**, 3170–3175 (2015).
[114] WHO, IARC Monograph on the Evaluation of Carcinogenic Risk to Humans **99**, 55–67 (2010).
[115] Y.-L. Sun, Z.-S. Hou, S.-M. Sun, B.-Y. Zheng, J.-F. Ku, W.-F. Dong, Q.-D. Chen, and H.-B. Sun, Sci. Rep. **5**, 12852 (2015).
[116] L. Labrador-Paez, K. Soler-Carracedo, M. Hernandez-Rodriguez, I. R. Martin, T. Carmon, and L. L. Martin, Opt. Express, **25**, 1165–1172 (2017).
[117] C. Linslal, M. Kailasnath, S. Mathew, T. Nideep, P. Radhakrishnan, V. Nampoori, and C. Vallabhan, Opt. Lett. **41**, 551–554 (2016).
[118] R. Chen, V. D. Ta, and H. Sun, ACS Photonics **1**, 11–16 (2014).
[119] Y. S. L. V. Narayana, D. Venkatakrishnarao, A. Biswas, M. A. Mohiddon, N. Viswanathan, and R. Chandrasekar, ACS Appl. Mater. Interfaces **8**, 952–958 (2016).
[120] X. Lin, Y. Fang, L. Zhu, J. Zhang, G. Huang, J. Wang, and Y. Mei, Adv. Opt. Mater. **4**, 936–942 (2016).
[121] S. Lacey, I. M. White, Y. Sun, S. I. Shopova, J. M. Cupps, P. Zhang, and X. Fan, Opt. Express. **15**, 15523–15530 (2007).
[122] V. Marx, Nat. Methods **12**, 187–190 (2015).
[123] L. Song, E. J. Hennik, I. T. Young, and H. J. Tanke, Biophys. J. **68**, 2588–2600 (1995).
[124] A. J. Kuehne and M. C. Gather, Chem. Rev. **116**, 12823–12864 (2016).
[125] S. Rochat and T. M. Swager, ACS Appl. Mater. Interfaces **5**, 4488–502 (2013).
[126] R. M. Ma, S. Ota, Y. Li, S. Yang, and X. Zhang, Nat. Nanotechnol. **9**, 600–4 (2014).
[127] K. Tabata, D. Braam, S. Kushida, L. Tong, J. Kuwabara, T. Kanbara, A. Beckel, A. Lorke, and Y. Yamamoto, Sci. Rep. **4**, 5902 (2014).
[128] S. Kushida, D. Braam, T. D. Dao, H. Saito, K. Shibasaki, S. Ishii, T. Nagao, A. Saeki, J. Kuwabara, T. Kanbara, M. Kijima, A. Lorke, and Y. Yamamoto, ACS Nano **10**, 5543–5549 (2016).
[129] A. J. Lam, F. St-Pierre, Y. Gong, J. D. Marshall, P. J. Cranfill, M. A. Baird, M. R. McKeown, J. Wiedenmann, M. W. Davidson, M. J. Schnitzer, R. Y. Tsien, and M. Z. Lin, Nat. Methods **9**, 1005–1012 (2012).
[130] L. Cerdan, E. Enciso, V. Martin, J. Banuelos, I. Lopez-Arbeloa, A. Costela, and I. Garcia-Moreno, Nat. Photon. **6**, 621–626 (2012).
[131] M. Berggren, A. Dodabalapur, R. E. Slusher, and Z. Bao, Nature **389**, 466–469 (1997).
[132] M. C. Gather and S. H. Yun, Nat. Photon. **5**, 406–410 (2011).
[133] A. Jonas, M. Aas, Y. Karadag, S. Manioglu, S. Anand, D. McGloin, H. Bayraktar, and A. Kiraz, Lab Chip **14**, 3093–3100 (2014).
[134] Y.-C. Chen, Q. Chen, and X. Fan, Lab Chip **16**, 2228–2235 (2016).
[135] A. Kiraz, Q. Chen, and X. Fan, ACS Photonics **2**, 707–713 (2015).
[136] C.-S. Wu, M. K. Khaing Oo, and X. Fan, ACS Nano **4**, 5897–5904 (2010).
[137] Y. Zhi, J. Valenta, and A. Meldrum, J. Opt. Soc. Am. B **30**, 3079–3085 (2013).
[138] S. Lane, P. West, A. François, and A. Meldrum, Opt. Express **23**, 2577–2590 (2015).
[139] X. Yang and B. Li, ACS Macro Lett. **3**, 1266–1270 (2014).
[140] R. S. Moirangthem and A. Erbe, Appl. Phys. Lett. **103**, 051108 (2013).
[141] C. Czekalla, C. Sturm, R. Schmidt-Grund, B. Cao, M. Lorenz, and M. Grundmann, Appl. Phys. Lett. **92**, 241102 (2008).
[142] A. Paunoiu, R. S. Moirangthem, and A. Erbe, Phys. Status Solidi RRL **9**, 241–244 (2015).
[143] M. V. Maximov, N. V. Kryzhanovskaya, A. M. Nadtochiy, E. I. Moiseev, I. I. Shostak, A. A. Bogdanov, Z. F. Sadrieva, A. E. Zhukov, A. A. Lipovskii, and D. V. Karpov, Nanoscale Res. Lett. **9**, 1–7 (2014).
[144] E. Stock, F. Albert, C. Hopfmann, M. Lermer, C. Schneider, S. Höfling, A. Forchel, M. Kamp, and S. Reitzenstein, Adv. Mater. **25**, 707–710 (2013).
[145] S. Shopova, G. Farca, A. Rosenberger, W. Wickramanayake, and N. Kotov, Appl. Phys. Lett. **85**, 6101–6103 (2004).
[146] W. K. Bae, Y.-S. Park, J. Lim, D. Lee, L. A. Padilha, H. McDaniel, I. Robel, C. Lee, J. M. Pietryga, and V. I. Klimov, Nat. Commun. **4**, 2661 (2013).
[147] V. I. Klimov, A. A. Mikhailovsky, D. W. McBranch, C. A. Leatherdale, and M. G. Bawendi, Science **287**, 1011–1013 (2000).
[148] C. Motta, F. El-Mellouhi, S. Kais, N. Tabet, F. Alharbi, and S. Sanvito, Nat. Commun. **6**, 7026 (2015).
[149] Q. Zhang, R. Su, X. Liu, J. Xing, T. C. Sum, and Q. Xiong, Adv. Funct. Mater. **26**, 6238–6245 (2016).
[150] K. Wang, S. Sun, C. Zhang, W. Sun, Z. Gu, S. Xiao, and Q. Song, arXiv preprint arXiv:1606.07542 (2016).
[151] L. Collot, V. Lefevre-Seguin, M. Brune, J. Raimond, and S. Haroche, EPL **23**, 327–334 (1993).

[152] D. Ristić, S. Berneschi, M. Camerini, D. Farnesi, S. Pelli, C. Trono, A. Chiappini, A. Chiasera, M. Ferrari, and A. Lukowiak, JOL **170**, 755–760 (2016).
[153] Y. Deng, R. K. Jain, and M. Hossein-Zadeh, Opt. Lett. **39**, 4458–4461 (2014).
[154] T. Kishi, T. Kumagai, S. Shibuya, F. Prudenzano, T. Yano, and S. Shibata, Opt. Express **23**, 20629–20635 (2015).
[155] C. Pérez-Rodríguez, L. Labrador-Páez, I. R. Martín, and S. Ríos, Laser Phys. Lett. **12**, 046003 (2015).
[156] S. Mehrabani and A. M. Armani, Opt. Lett. **38**, 4346–4349 (2013).
[157] T. Lu, L. Yang, R. V. A. van Loon, A. Polman, and K. J. Vahala, Opt. Lett. **34**, 482–484 (2009).
[158] Q. Li, Y. Huang, Y. Lin, J. Wu, J. Huang, and T. Wu, Opt. Commun. **356**, 368–372 (2015).
[159] V. Lefevre-Seguin, Opt. Mater. **11**, 153–165 (1999).
[160] A. Pal, S. Y. Chen, R. Sen, T. Sun, and K. Grattan, Laser Phys. Lett. **10**, 085101 (2013).
[161] R. Lessard, O. Rousseau-Cyr, M. Charlebois, C. Riviere, O. Mermut, and C. N. Allen, Proc. SPIE **8600**, 86001Q1–86001Q8 (2013).
[162] X. Fan and S.-H. Yun, Nat. Method **11**, 141–147 (2014).
[163] A. Ashkin and J. M. Dziedzic, Phys. Rev. Lett. **38**, 1351–1354 (1977).
[164] S. Uetake, R. S. D. Sihombing, and K. Hakuta, Opt. Lett. **27**, 421–423 (2002).
[165] S. K. Y. Tang, R. Derda, Q. Quan, M. Lončar, and G. M. Whitesides, Opt. Express **19**, 2204–2215 (2011).
[166] S. Anand, M. Eryürek, Y. Karadag, A. Erten, A. Serpengüzel, A. Jonáš, and A. Kiraz, J. Opt. Soc. Am. B **33**, 1349–1354 (2016).
[167] I. Muševič, Liq. Cryst. Rev. **4**, 1–34 (2016).
[168] T. A. Kumar, M. A. Mohiddon, N. Dutta, N. K. Viswanathan, and S. Dhara, Appl. Phys. Lett. **106**, 051101 (2015).
[169] V. D. Ta, R. Chen, and H. D. Sun, Sci. Rep. **3**, 1362 (2013).
[170] S. Yang, Y. Wang, R. Chen, T. He, H. V. Demir, and H. Sun, Sci. Rep. **6**, 27200 (2016).
[171] A. B. Petermann, A. Varkentin, B. Roth, U. Morgner, and M. Meinhardt-Wollweber, Opt. Express **24**, 6052–6062 (2016).
[172] C. Wei, M. Gao, F. Hu, J. Yao, and Y. S. Zhao, Adv. Opt. Mater. **4**, 1009–1014 (2016).
[173] M. Himmelhaus, Optik Photonik **11**, 43–47 (2016).
[174] S. Kushida, D. Braam, C. Pan, T. D. Dao, K. Tabata, K. Sugiyasu, M. Takeuchi, S. Ishii, T. Nagao, A. Lorke, and Y. Yamamoto, Macromolecules **48**, 3928–3933 (2015).
[175] P. G. Schiro and A. S. Kwok, Opt. Express **12**, 2857–2863 (2004).
[176] H. Li, S. Hao, L. Qiang, J. Li, and Y. Zhang, Appl. Phys. Lett. **102**, 231908 (2013).
[177] K. Kosma, G. Zito, K. Schuster, and S. Pissadakis, Opt. Lett. **38**, 1301–1303 (2013).
[178] Y. Liu, M. Luo, Z. Wang, Z. Li, W.-Y. Zhou, J. Guo, W. Huang, and X. Liu, J. Lightwave Technol. **99**, 1–6 (2016).
[179] A. François, K. J. Rowland, V. S. Afshar, M. R. Henderson, and T. M. Monro, Opt. Express **21**, 22566–22577 (2013).
[180] L. Martín, D. Navarro-Urrios, F. Ferrarese-Lupi, C. Pérez-Rodríguez, I. Martín, J. Montserrat, C. Domínguez, B. Garrido, and N. Capuj, Laser Phys. **23**, 075801 (2013).
[181] T. Kumagai, T. Kishi, and T. Yano, J. Appl. Phys. **117**, 113104 (2015).
[182] A. K. Bhowmik, Appl. Opt. **39**, 3071–3075 (2000).
[183] B. Gayral, J. M. Gérard, A. Lemaître, C. Dupuis, L. Manin, and J. L. Pelouard, Appl. Phys. Lett. **75**, 1908–1910 (1999).
[184] A. L. Washburn, L. C. Gunn, and R. C. Bailey, Anal. Chem. **81**, 9499–9506 (2009).
[185] M. Ghulinyan, A. Pitanti, G. Pucker, and L. Pavesi, Opt. Express **17**, 9434–9441 (2009).
[186] A. M. Flatae, M. Burresi, H. Zeng, S. Nocentini, S. Wiegele, C. Parmeggiani, H. Kalt, and D. Wiersma, Light Sci. Appl. **4**, e282 (2015).
[187] V. N. Astratov, Photonic Microresonator Research, and Applications, Vol. 156 (Springer, 2010), p. 423–457.
[188] M. Li, N. Zhang, K. Wang, J. Li, S. Xiao, and Q. Song, Sci. Rep. **5**, 13682 (2015).
[189] L. X. Zou, Y. Z. Huang, X. M. Lv, X. W. Ma, J. L. Xiao, Y. De Yang, and Y. Du, Electron. Lett. **51**, 1442–1443 (2015).
[190] H. Chandrahalim, S. C. Rand, and X. Fan, Sci. Rep. **6**, 32668 (2016).
[191] C. P. K. Manchee, V. Zamora, J. W. Silverstone, J. G. C. Veinot, and A. Meldrum, Opt. Express **19**, 21540–21551 (2011).
[192] S. Lane, J. Chan, T. Thiessen, and A. Meldrum, Sens. Actuator B-Chem. **190**, 752–759 (2014).
[193] O. G. Schmidt and K. Eberl, Nature **410**, 168–168 (2001).
[194] C. Vervacke, C. C. Bof Bufon, D. J. Thurmer, and O. G. Schmidt, RSC Advances **4**, 9723–9729 (2014).
[195] G. Huang, V. A. Bolaños Quiñones, F. Ding, S. Kiravittaya, Y. Mei, and O. G. Schmidt, ACS Nano **4**, 3123–3130 (2010).
[196] J. Zhang, J. Zhong, Y. F. Fang, J. Wang, G. S. Huang, X. G. Cui, and Y. F. Mei, Nanoscale **6**, 13646–13650 (2014).
[197] S. Tang, Y. Fang, Z. Liu, L. Zhou, and Y. Mei, Lab Chip **16**, 182–187 (2016).
[198] J. L. Nadeau, V. S. Ilchenko, D. Kossakovski, G. H. Bearman, and L. Maleki, "High-Q whispering-gallery mode sensor in liquids," Proc. SPIE **4629**, 172–180 (2002).
[199] C.-Y. Chao and L. J. Guo, J. Lightwave Technol. **24**, 1395–1402 (2006).
[200] X. Zhou, L. Zhang, and W. Pang, Opt. Express **24**, 18197–18208 (2016).
[201] L. Martin, S. León-Luis, C. Pérez-Rodríguez, I. Martín, U. Rodríguez-Mendoza, and V. Lavín, J. Opt. Soc. Am. B **30**, 3254–3259 (2013).
[202] A. H. Zamanian and T. Ioppolo, Appl. Opt. **54**, 7124–7130 (2015).
[203] M. Manzo and T. Ioppolo, Opt. Lett. **40**, 2257–2260 (2015).
[204] J. M. Ward, Y. Yang, and S. N. Chormaic, Sci. Rep. **6**, 25152 (2016).
[205] J. Hernández, and I. M. Thompson, Cancer **101**, 894–904 (2004).
[206] K. R. Kozak, F. Su, J. P. Whitelegge, K. Faull, S. Reddy, and R. Farias-Eisner, Proteomics **5**, 4589–4596 (2005).
[207] S. Arnold, M. Khoshsima, I. Teraoka, S. Holler, and F. Vollmer, Opt. Lett. **28**, 272–274 (2003).
[208] H. Zhu, I. M. White, J. D. Suter, P. S. Dale, and X. Fan, Opt. Express **15**, 9139–9146 (2007).
[209] H. T. Beier, G. L. Coté, and K. E. Meissner, J. Opt. Soc. Am. B **27**, 536–543 (2010).

[210] I. M. White and X. Fan, Opt. Express **16**, 1020–1028 (2008).
[211] S. V. Boriskina, J. Opt. Soc. Am. B **23**, 1565–1573 (2006).
[212] L. Ren, X. Wu, M. Li, X. Zhang, L. Liu, and L. Xu, Opt. Lett. **37**, 3873–3875 (2012).
[213] V. D. Ta, R. Chen, and H. Sun, Adv. Opt. Mater **2**, 220–225 (2014).
[214] H. A. Huckabay, S. M. Wildgen, and R. C. Dunn, Biosens. Bioelectron. **45**, 223–229 (2013).
[215] G. Nunzi Conti, S. Berneschi, and S. Soria, Biosensors **6**, 1–11 (2016).
[216] F. Vollmer and L. Yang, Nanophotonics **1**, 267–291 (2012).
[217] E. Nuhiji and P. Mulvaney, Small **3**, 1408–1414 (2007).
[218] T. Reynolds, A. François, N. Riesen, M. E. Turvey, S. J. Nicholls, P. Hoffmann, and T. M. Monro, Anal. Chem. **88**, 4036–4040 (2016).
[219] C.-Y. Chao, W. Fung, and L. J. Guo, IEEE J. Sel. Top. Quantum Electron. **12**, 134–142 (2006).
[220] T. Beck, M. Mai, T. Grossmann, T. Wienhold, M. Hauser, T. Mappes, and H. Kalt, Appl. Phys. Lett. **102**, 121108 (2013).
[221] U. Bog, F. Brinkmann, H. Kalt, C. Koos, T. Mappes, M. Hirtz, H. Fuchs, and S. Köber, Small **10**, 3863–3868 (2014).
[222] J. Chan, T. Thiessen, S. Lane, P. West, K. Gardner, A. François, and A. Meldrum, IEEE Sens. J. **15**, 3467–3474 (2015).
[223] Ş. K. Özdemir, J. Zhu, X. Yang, B. Peng, H. Yilmaz, L. He, F. Monifi, S. H. Huang, G. L. Long, and L. Yang, Proc. Natl. Acad. Sci. **111**, 3836–3844 (2014).
[224] F. Wang, M. Anderson, M. T. Bernards, and H. K. Hunt, Sensors **15**, 18040–18060 (2015).
[225] L. Pasquardini, S. Berneschi, A. Barucci, F. Cosi, R. Dallapiccola, M. Insinna, L. Lunelli, G. N. Conti, C. Pederzolli, and S. Salvadori, J. Biophotonics **6**, 178–187 (2013).
[226] S. Spindel and K. E. Sapsford, Sensors **14**, 22313–22341 (2014).
[227] J. M. Humphries, M. A. Penno, F. Weiland, M. Klingler-Hoffmann, A. Zuber, A. Boussioutas, M. Ernst, and P. Hoffmann, Biochim. Biophys. Acta **1844**, 1051–1058 (2014).
[228] F. Vollmer, S. Arnold, D. Braun, I. Teraoka, and A. Libchaber, Biophys. J. **85**, 1974–1979 (2003).
[229] I. A. Estrada, R. W. Burlingame, A. P. Wang, K. Chawla, T. Grove, J. Wang, S. O. Southern, M. Iqbal, L. C. Gunn, and M. A. Gleeson, Proc. SPIE **9490**, 94900E1–94900E14 (2015).
[230] H. A. Huckabay and R. C. Dunn, Sens. Actuators B **160**, 1262–1267 (2011).
[231] Y. Sun and X. Fan, Angew. Chem. Int. Ed. **51**, 1236–1239 (2012).
[232] Q. Chen, M. Ritt, S. Sivaramakrishnan, Y. Sun, and X. Fan, Lab Chip **14**, 4590–4595 (2014).
[233] F. Wu, Y. Wu, Z. Niu, and F. Vollmer, Sensors **16**, 1197 (2016).
[234] B. Min, E. Ostby, V. Sorger, E. Ulin-Avila, L. Yang, X. Zhang, and K. Vahala, Nature **457**, 455–458 (2009).
[235] C. D. Geddes, Metal-enhanced fluorescence (John Wiley & Sons, 2010).
[236] C.-J. Huang, J. Dostalek, A. Sessitsch, and W. Knoll, Anal. Chem. **83**, 674–677 (2011).
[237] L. K. Ausman and G. C. Schatz, J. Chem. Phys. **129**, 054704 (2008).
[238] I. M. White, H. Oveys, and X. Fan, Spectroscopy **21**, 36–42 (2006).
[239] R.-S. Liu, W.-L. Jin, X.-C. Yu, Y.-C. Liu, and Y.-F. Xiao, Phys. Rev. A **91**, 043836 (2015).
[240] Y. Hu, L. Shao, S. Arnold, Y.-C. Liu, C.-Y. Ma, and Y.-F. Xiao, Phys. Rev. A **90**, 043847 (2014).
[241] L. Shao, X. F. Jiang, X. C. Yu, B. B. Li, W. R. Clements, F. Vollmer, W. Wang, Y. F. Xiao, and Q. Gong, Adv. Mater. **25**, 5616–5620 (2013).
[242] Y.-C. Chen, Q. Chen, and X. Fan, Optica **3**, 809–815 (2016).
[243] S. Yang, Y. Wang, Y. Gao, T. He, R. Chen, H. V. Demir, and H. Sun, Appl. Phys. Lett. **107**, 221103 (2015).
[244] M. Iqbal, R. W. Burlingame, R. Romero, A. Wang, T. Grove, and M. A. Gleeson, Label-Free Biosensor Methods in Drug Discovery (Spring, New York, 2015), p. 133–153.
[245] M. Saito, H. Shimatani, and H. Naruhashi, Opt. Express **16**, 11915–11919 (2008).
[246] K. J. Rowland, A. François, P. Hoffmann, and T. M. Monro, Opt. Express **21**, 11492–11505 (2013).
[247] M. Humar, M. C. Gather, and S.-H. Yun, Opt. Express **23**, 27865–27879 (2015).
[248] D. Venkatakrishnarao and R. Chandrasekar, Adv. Opt. Mater. **4**, 112–119 (2016).
[249] J. Li, Y. Lin, J. Lu, C. Xu, Y. Wang, Z. Shi, and J. Dai, ACS Nano **9**, 6794–6800 (2015).
[250] K. Okazaki, T. Shimogaki, K. Fusazaki, M. Higashihata, D. Nakamura, N. Koshizaki, and T. Okada, Appl. Phys. Lett. **101**, 211105 (2012).
[251] S.-H. Gong, S.-M. Ko, M.-H. Jang, and Y.-H. Cho, Nano Lett. **15**, 4517–4524 (2015).
[252] Y. Wang, K. S. Leck, V. D. Ta, R. Chen, V. Nalla, Y. Gao, T. He, H. V. Demir, and H. Sun, Adv. Mater. **27**, 169–175 (2015).
[253] S. W. Eaton, M. Lai, N. A. Gibson, A. B. Wong, L. Dou, J. Ma, L.-W. Wang, S. R. Leone, and P. Yang, Proc. Natl. Acad. Sci. **113**, 1993–1998 (2016).
[254] Q. Liao, K. Hu, H. Zhang, X. Wang, J. Yao, and H. Fu, Adv. Mater. **27**, 3405–3410 (2015).
[255] X.-F. Liu, F. Lei, M. Gao, X. Yang, C. Wang, Ş. K. Özdemir, L. Yang, and G.-L. Long, Opt. Express **24**, 9550–9560 (2016).
[256] F. Sedlmeir, R. Zeltner, G. Leuchs, and H. G. Schwefel, Opt. Express **22**, 30934–30942 (2014).
[257] S. Berneschi, D. Farnesi, F. Cosi, G. N. Conti, S. Pelli, G. Righini, and S. Soria, Opt. Lett. **36**, 3521–3523 (2011).
[258] H. Zhu, I. M. White, J. D. Suter, M. Zourob, and X. Fan, Anal. Chem. **79**, 930–937 (2007).
[259] Y. Zhi, C. Manchee, J. Silverstone, Z. Zhang, and A. Meldrum, Plasmonics **8**, 71–78 (2013).
[260] V. Zamora, A. DÝez, M. V. AndrÚs, and B. Gimeno, Opt. Express **15**, 12011–12016 (2007).
[261] H. Li and X. Fan, Appl. Phys. Lett. **97**, 011105 (2010).
[262] X. Zhang, L. Ren, X. Wu, H. Li, L. Liu, and L. Xu, Opt. Express **19**, 22242–22247 (2011).